

The thermal properties of porous andesite

Michael J. Heap ^{a,*}, Alexandra R.L. Kushnir ^a, Jérémie Vasseur ^b, Fabian B. Wadsworth ^c, Pauline Harlé ^a, Patrick Baud ^a, Ben M. Kennedy ^d, Valentin R. Troll ^e, Frances M. Deegan ^e

^a Géophysique Expérimentale, Institut de Physique de Strasbourg (UMR 7516 CNRS, Université de Strasbourg/EOST), 5 rue René Descartes, 67084 Strasbourg cedex, France

^b Earth and Environmental Sciences, Ludwig-Maximilians-Universität, Theresienstrasse 41, 80333 Munich, Germany

^c Department of Earth Sciences, Science Labs, Durham University, Durham DH1 3LE, UK

^d Department of Geological Sciences, University of Canterbury, Private Bag 4800, Christchurch 8140, New Zealand

^e Department of Earth Sciences, Section for Natural Resources and Sustainable Development (NRHU), Villavägen 16, Uppsala University, 752 36 Uppsala, Sweden

ARTICLE INFO

Article history:

Received 11 February 2020

Received in revised form 15 April 2020

Accepted 21 April 2020

Available online 29 April 2020

Keywords:

Thermal conductivity

Thermal diffusivity

Specific heat capacity

Andesite

Porosity

Hydrothermal alteration

ABSTRACT

The thermal properties of volcanic rocks are crucial to accurately model heat transfer in volcanoes and in geothermal systems located within volcanic deposits. Here we provide laboratory measurements of thermal conductivity and thermal diffusivity for variably porous andesites from Mt. Ruapehu (New Zealand) and variably altered basaltic-andesites from Merapi volcano (Indonesia) measured at ambient laboratory pressure and temperature using the transient hot-strip method. The specific heat capacity of each sample was then calculated using these measured values and the bulk sample density. Thermal conductivity and thermal diffusivity decrease as a function of increasing porosity, but specific heat capacity does not vary systematically with porosity. For a given porosity, saturation with water increases thermal conductivity and specific heat capacity, but decreases thermal diffusivity. Measurements on samples from Merapi volcano show that, compared to the unaltered samples from Mt. Ruapehu, hydrothermal alteration deceases thermal conductivity and thermal diffusivity, and increases specific heat capacity. We use an effective medium approach to parameterise these data, showing that when the porosity and pore-fluid properties are scaled for, the measured values agree well with theoretical predictions. We find that despite the microstructural complexity of the studied andesites, porosity is the principal parameter dictating their thermal properties. To understand whether the measured changes in thermal properties are sufficient to influence natural processes, we model heat transfer from magma to the surrounding host-rock by solving Fick's second law cast in 1D Cartesian (dyke geometry) and cylindrical (conduit geometry) coordinates. We provide models for different host-rock porosities (0–0.6), different initial magmatic temperatures (800–1200 °C), and different levels of host-rock alteration. Our modelling shows how the cooling of a dyke and conduit is slowed by a higher host-rock porosity and by increased hydrothermal alteration. The thermal properties provided herein can help improve modelling designed to inform on volcanic and geothermal processes.

© 2020 Elsevier B.V. All rights reserved.

1. Introduction

Volcanic systems are thermally dynamic environments (e.g., Oppenheimer et al., 1993; Harris et al., 1997; Harris and Stevenson, 1997; Wright et al., 2004; Hutchison et al., 2013; Heap et al., 2018). As a result, the thermal properties of volcanic rocks are an important input parameter for a wide range of predictive models. Examples include: the modelling of heat loss from lava flows, pyroclastic density current deposits, dykes, sills, conduits, and magma chambers (e.g., Irvine, 1970; Norton and Knight, 1977; Carrigan, 1984; Bruce and Huppert, 1989; Carrigan et al., 1992; Fialko and Rubin, 1999; Bagdassarov and Dingwell, 1994; Wooster et al., 1997; Annen et al.,

2008; Nabelek et al., 2012; Heap et al., 2014; Schauroth et al., 2016; Heap et al., 2017a; Annen, 2017; Mattsson et al., 2018; Tsang et al., 2019), the modelling of the internal structure and hydrological system of volcanoes (e.g., Sammel et al., 1988; Ehara, 1992; Violette et al., 1997; Hurwitz et al., 2002, 2003; De Natale et al., 2004), ground deformation modelling (e.g., Del Negro et al., 2009; Currenti et al., 2010; Fournier and Chardot, 2012), outgassing models (e.g., Chioldini et al., 2001), models of viscous sintering (e.g., Wadsworth et al., 2014), and heat transfer in volcanic lightning storms (e.g., Wadsworth et al., 2017). In addition, the thermal properties of volcanic rocks are also of use in modelling designed to better understand large-scale fluid circulation, heat flow calculations, and temperature estimations at volcanic geothermal sites, such as those in Iceland (e.g., Bodvarsson et al., 1984; Flóvenz and Saemundsson, 1993) and New Zealand (e.g., Mercer and Faust, 1979; Kühn and Stöfen, 2005). Finally, an

* Corresponding author.

E-mail address: heap@unistra.fr (M.J. Heap).



understanding of the thermal properties of volcanic rocks is important due to their influence on permeability-enhancing thermal fracturing (e.g., Bauer and Handin, 1983; Siratovich et al., 2015; Lamur et al., 2018).

Due to the need for robust parameters for modelling, experimental studies have provided values of the thermal properties of volcanic rocks (e.g., Horai et al., 1970; Fujii and Osako, 1973; Robertson and Peck, 1974; Bagdassarov and Dingwell, 1994; Whittington et al., 2009; Romine et al., 2012; Mielke et al., 2015, 2016, 2017; Vélez et al., 2018; Hofmeister, 2019). Robertson and Peck (1974), for example, calculated the thermal conductivity of variably porous basalt from Hawai'i (USA) using the steady-state method. These authors found that thermal conductivity decreased from $\sim 1.7 \text{ W}\cdot\text{m}^{-1}\cdot\text{K}^{-1}$ at a porosity <0.05 to $\sim 0.2 \text{ W}\cdot\text{m}^{-1}\cdot\text{K}^{-1}$ at a porosity of ~ 0.85 . Romine et al. (2012) found that the thermal diffusivity of rhyolite from Mono Craters (USA), measured using the laser-flash analysis method, decreased from ~ 0.65 to $\sim 0.55 \text{ mm}^2\cdot\text{s}^{-1}$ as temperature was increased from ~ 20 to $\sim 430^\circ\text{C}$, but remained constant from ~ 430 to $\sim 1300^\circ\text{C}$. These authors also calculated that the thermal conductivity of rhyolitic glasses and melts increases from ~ 1.1 to $\sim 1.5 \text{ W}\cdot\text{m}^{-1}\cdot\text{K}^{-1}$ as temperature is increased from ~ 20 to $\sim 1300^\circ\text{C}$. Horai et al. (1970) and Fujii and Osako (1973) found that the thermal diffusivity of lunar basalt, measured using the modified Ångström method, decreased from ~ 0.7 to $\sim 0.5 \text{ mm}^2\cdot\text{s}^{-1}$ as temperature was increased from ~ 20 to $\sim 230^\circ\text{C}$. Mielke et al. (2015) measured the thermal properties of volcanic rocks (andesites and rhyolites) from the Tauhara geothermal field (New Zealand) using a portable device that measures thermal conductivity and thermal diffusivity using a modified optical scanning method. For example, they found average thermal conductivities of 1.32 and $1.11 \text{ W}\cdot\text{m}^{-1}\cdot\text{K}^{-1}$ for andesite lava (average porosity = 0.095) and rhyolite lava (average porosity = 0.275), respectively. Mielke et al. (2016) measured the thermal properties of volcanic rocks (andesite, dacite, and rhyolite) from the Taupō Volcanic Zone (New Zealand) using the optical scanning method. The thermal conductivities of the andesite (porosity = 0.023–0.130), dacite (porosity = 0.108), and rhyolite (porosity = 0.231) samples were $1.19\text{--}1.70$, 1.18 , and $1.04 \text{ W}\cdot\text{m}^{-1}\cdot\text{K}^{-1}$, respectively. Despite these studies, there is a paucity of thermal property data (thermal conductivity, thermal diffusivity, and specific heat capacity) for volcanic rocks spanning a wide porosity range. These data are necessary to test effective medium expressions which, if found to well describe data for volcanic rocks, can be used in a variety of modelling approaches.

We report here on measurements of thermal conductivity, thermal diffusivity, and specific heat capacity for variably porous (porosity from 0.02 to 0.628) andesites from Mt. Ruapehu (Taupō Volcanic Zone); we additionally assess the role of water-saturation on the thermal properties of these andesite samples. Due to the ubiquity of hydrothermally altered zones at active volcanoes worldwide (e.g., Rosas-Carabal et al., 2016; Byrdina et al., 2017; Heap et al., 2017b), we also investigated the influence of hydrothermal alteration on thermal properties by measuring a suite of variably altered basaltic-andesite samples from Merapi volcano (Indonesia). Theoretical predictions were then tested against these data. Finally, to understand whether the measured changes in thermal properties are sufficient to influence natural processes, we modelled the cooling of a dyke and a conduit by solving the heat equation in 1D in Cartesian and cylindrical coordinates, respectively. We provide models that cover a range of typical situations; namely, for different host-rock porosities (0, 0.3, and 0.6), different initial magmatic temperatures (800 , 1000 , and 1200°C), and different alteration intensities.

2. Experimental materials and methods

Two suites of rocks were measured: (1) variably porous andesites from Mt. Ruapehu and (2) variably altered basaltic-andesites from Merapi volcano.

The andesites from Mt. Ruapehu (Taupō Volcanic Zone; see reviews by Graham et al., 1995; Wilson et al., 1995) were collected on the northern flank of the volcano (from the Whakapapa Formation; Hackett and Houghton, 1989). The blocks were collected thanks to a permit obtained through the Department of Conservation (DOC) and following consultation with the Māori Iwi. The andesites from Mt. Ruapehu are porphyritic in texture and contain large phenocrysts of plagioclase and pyroxene in a glassy groundmass containing abundant microlites (Fig. 1a–c; Heap and Kennedy, 2016). In total, 17 blocks of andesite were collected and labelled from R1 to R17 (labels used here are the same as in Heap and Kennedy, 2016). Apart from the presence of rare pore-filling cristobalite in four of the low-porosity samples (indicated in Tables 2 and 3), the blocks from Mt. Ruapehu are not visibly altered (from hand-sample inspection and microstructural observations; see Heap and Kennedy, 2016). The porosity of the samples comprises both pores and microcracks (Fig. 1a–c).

The basaltic-andesites from Merapi volcano (Indonesia; Voight et al., 2000; Surono et al., 2012; Kushnir et al., 2016), collected from the summit area of the volcano (from the 1902 lava dome, about 100 m to the northeast of the currently active dome), are characterised by a porphyritic texture comprising phenocrysts of dominantly plagioclase and pyroxene within a crystallised groundmass (plagioclase, K-feldspar, and pyroxene; Fig. 1d–e; see Heap et al., 2019a). In total, five blocks of basaltic-andesite were collected and classified in terms of their alteration (based on the wt% of alteration minerals determined by X-ray powder diffraction; Table 1; Heap et al., 2019a). The alteration phases present, indicative of exposure to acid-sulfate fluids, include natroalunite, alunite, quartz, hematite, cristobalite, gypsum, and unclassified amorphous phases (Fig. 1d–e; Table 1; Heap et al., 2019a). The five blocks from Merapi volcano were labelled M-U ("unaltered"), M-SA1 and M-SA2 ("slightly altered"), and M-HA1 and M-HA2 ("highly altered"). The labels for these materials are the same as in Heap et al. (2019a). The porosity of the samples comprises both pores and microcracks (Fig. 1d–e).

Multiple cylindrical samples, 20 mm in diameter, were cored from the blocks collected and their ends were cut and ground flat and parallel to a nominal length of 40 mm. These samples were then dried under vacuum at 40°C for at least 48 h. The dry bulk sample density was measured for each sample using the dry mass and the bulk sample volume determined using the sample dimensions. The connected porosities of the cylindrical samples were calculated using the skeletal volume measured by a helium pycnometer (Micromeritics AccuPyc II 1340) and the bulk sample volume.

The thermal conductivity, λ (in $\text{W}\cdot\text{m}^{-1}\cdot\text{K}^{-1}$), and thermal diffusivity, D (in $\text{mm}^2\cdot\text{s}^{-1}$), of each sample was measured using a Hot Disk TPS 500 Thermal Constants Analyser using the transient plane source (TPS) method (outlined in Gustafsson, 1991; Gustavsson et al., 1994; Harlé et al., 2019). The TPS method is a periodic method of thermal property measurement (see the review by Hofmeister, 2019). The standard uncertainty for values of thermal conductivity and thermal diffusivity using the transient hot-strip method has been determined to be 2.6 and 11%, respectively (Hammerschmidt and Sabuga, 2000). Measurement uncertainty using this technique arises from contact losses and ballistic radiative transfer gains (Hofmeister, 2019).

A sensor consisting of two $10 \mu\text{m}$ -thick nickel foil spirals (radius = 3.189 mm) insulated on both sides by $30 \mu\text{m}$ -thick kapton (Fig. 2, inset) was sandwiched between the cylindrical sample and a piece of polyurethane foam of known thermal properties (Fig. 2). The sample and foam piece were held in place using a screw positioned at the top of the sample jig (Fig. 2), which ensured good contact between the surface of the sample and the sensor. The temperature adjacent to the sample was measured using a thermocouple and was inputted into the system prior to launching each measurement. During the measurement, an electrical current of known power and duration was passed through the sensor, which also recorded the increase in sample temperature as a function of time. The output power and duration required for a reliable

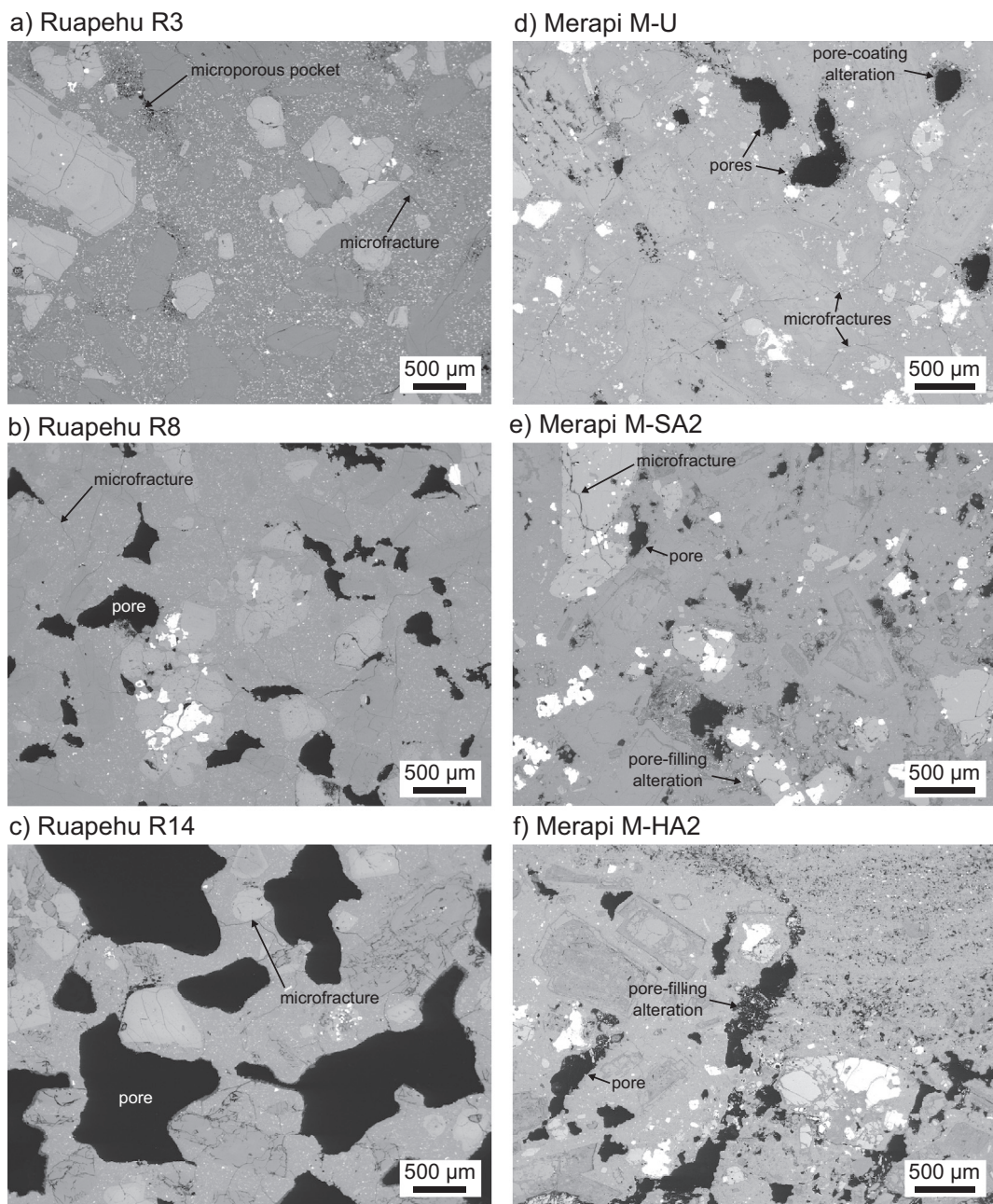


Fig. 1. Backscattered scanning electron microscope images of select samples from Ruapehu (panels a to c; images from Heap and Kennedy (2016)) and Merapi (panels d to e; images from Heap et al. (2019a)). Important microstructural features are labelled on the images.

Table 1

X-ray powder diffraction (XRPD) analysis showing quantitative bulk mineralogical composition for the five blocks from Merapi volcano (in wt%). The five blocks from Merapi volcano are labelled M-U ("unaltered"), M-SA1 and M-SA2 ("slightly altered"), and M-HA1 and M-AH2 ("highly altered") (as in Heap et al., 2019a). An asterisk denotes an alteration phase. Data from Heap et al. (2019a).

Mineral	M-U	M-SA1	M-SA2	M-HA1	M-HA2
Plagioclase	54 ± 3	47 ± 3	38 ± 3	38 ± 3	19 ± 3
K-Feldspar	19 ± 3	9 ± 3	13 ± 3	6 ± 3	10 ± 3
Clinopyroxene ± orthopyroxene	16 ± 2	13 ± 2	14 ± 2	11 ± 2	8 ± 2
Magnetite	3 ± 0.5	2 ± 0.5	2.5 ± 0.5	<1 ± 0.5	<1 ± 0.5
Gypsum*	–	0.5 ± 0.5	4 ± 0.5	5 ± 0.5	6 ± 0.5
K-Na-Alunite*	–	1 ± 0.5	8.5 ± 2	11 ± 2	24 ± 2
Quartz*	1 ± 0.5	1.5 ± 0.5	0.5 ± 0.5	1 ± 0.5	0.5 ± 0.5
Hematite*	0.5 ± 0.5	2 ± 0.5	0.5 ± 0.5	3 ± 0.5	1 ± 0.5
Cristobalite*	6 ± 0.5	–	–	–	2.5 ± 0.5
Amorphous phases*	–	24 ± 4	19 ± 4	25 ± 4	28 ± 4

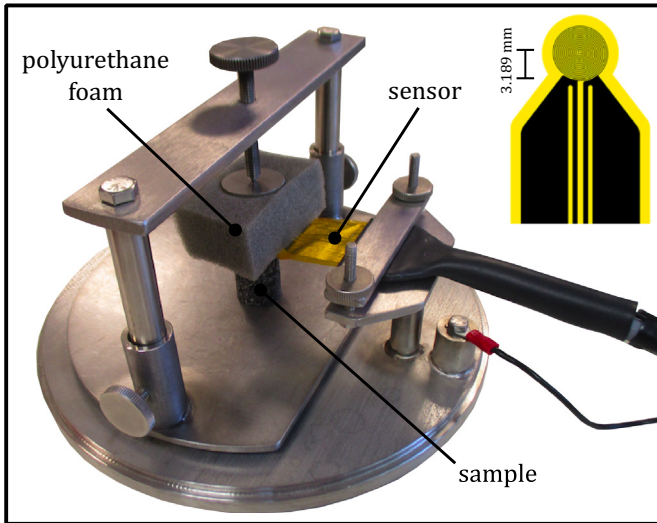


Fig. 2. Photograph of the experimental setup. The inset shows the detail of the sensor, consisting of two 10 μm -thick nickel foil spirals (radius = 3.189 mm) insulated on both sides by 30 μm -thick kapton.

measurement varied from sample to sample and were found using trial-and-error. Four consecutive measurements were performed on each sample and we report herein an average of these four measurements (standard deviations are provided in [Tables 2 and 3](#)). Each measurement was performed at least five min apart to ensure that the sample had cooled back to the ambient temperature. The sensor measured the temperature drift of the sample for 40 s prior to each measurement to check whether the sample was in thermal equilibrium. If the sample temperature was not constant during this 40 s period, the data were not considered and the measurement was repeated. “Wet” measurements were performed on samples saturated under vacuum with deionised water, a method that ensures the complete saturation of the connected void space. The wet mass of these samples was first measured in order to calculate the bulk sample density of the water-saturated samples. To perform the wet thermal property measurements, the entire jig ([Fig. 2](#)) was submersed in a water bath. Wet measurements were performed with the sensor sandwiched between two cylindrical samples cored from the same block (of identical or very similar porosity) of material, rather than using the polyurethane foam described above. The specific heat per unit volume, $\rho_b C_p$ (in $\text{J}/\text{m}^3\text{K}$), provided by the Hot Disk device was divided by the bulk sample density, ρ_b , to provide the bulk sample specific heat capacity, C_p (in $\text{kJ}\cdot\text{kg}^{-1}\cdot\text{K}^{-1}$). All measurements were conducted in a far-field environment that was at ambient laboratory temperature (ranging from 19 to 27 °C for the dry measurements and 18 to 20 °C for the wet measurements) and pressure (~100,000 Pa).

3. Results

Bulk sample density, specific heat capacity, and thermal conductivity are plotted as a function of connected porosity in [Fig. 3](#) (data available in [Tables 2 and 3](#)). We first note that bulk sample density decreases linearly as a function of increasing porosity for the dry samples from Mt. Ruapehu (black circles in [Fig. 3a](#)), suggesting that the volume of isolated porosity is constant over the porosity range or that the volume of isolated porosity in the studied samples is negligible. Although the bulk density of the dry samples from Merapi volcano decreases as a function of increasing porosity (green squares in [Fig. 3a](#)), the trend is much more scattered than that for the dry Mt. Ruapehu samples.

The specific heat capacity of the dry Mt. Ruapehu samples varies between 0.591 and 0.856 $\text{kJ}\cdot\text{kg}^{-1}\cdot\text{K}^{-1}$, but does not vary systematically with porosity (black circles in [Fig. 3b](#); [Table 2](#)). The specific heat capacity of the samples from Merapi volcano also does not vary systematically with porosity (green squares in [Fig. 3b](#)).

The thermal conductivity of the dry Mt. Ruapehu (black circles in [Fig. 3c](#)) and Merapi volcano (green squares in [Fig. 3c](#)) samples decreases as a function of increasing porosity. For example, at low porosity (<0.05), the thermal conductivity of the dry samples from Mt. Ruapehu is between ~1.4 and ~1.6 $\text{W}\cdot\text{m}^{-1}\cdot\text{K}^{-1}$, but is as low as ~0.4 $\text{W}\cdot\text{m}^{-1}\cdot\text{K}^{-1}$ when the porosity is ~0.6 ([Fig. 3c](#)).

The thermal diffusivity of the dry Mt. Ruapehu (black circles in [Fig. 4](#)) and Merapi volcano (green squares in [Fig. 4](#)) samples decreases as a function of increasing porosity, but the trend is more scattered than that for the thermal conductivity ([Fig. 3c](#)). For example, the thermal diffusivity of the dry samples from Mt. Ruapehu decreases from ~0.7–0.8 to ~0.5–0.55 $\text{mm}^2\cdot\text{s}^{-1}$ as porosity increases from <0.05 to ~0.6 ([Fig. 4](#)).

When saturated with water, the bulk density ([Fig. 3a](#)), specific heat capacity ([Fig. 3b](#)), and thermal conductivity ([Fig. 3c](#)) of the andesites from Mt. Ruapehu increased, and the thermal diffusivity decreased, relative to the dry state ([Fig. 4](#)). Our data also show that the influence of water saturation on the thermal properties of the andesites from Mt. Ruapehu depends on the porosity ([Fig. 5](#)). At low porosity (<0.05), the dry and wet thermal properties are essentially equal, but, at the maximum porosity of ~0.6, the specific heat capacity and thermal conductivity increased by a factor of ~4.5 and ~2.25, respectively ([Fig. 5a](#) and [c](#)), and the thermal diffusivity decreased by a factor of ~0.5 ([Fig. 5c](#)).

For a given porosity, the dry altered basaltic-andesites from Merapi volcano (green squares) have a higher density ([Fig. 3a](#)), a higher specific heat capacity ([Fig. 3b](#)), and a lower thermal conductivity ([Fig. 3c](#)) and thermal diffusivity ([Fig. 4](#)) than the dry andesites from Mt. Ruapehu. For example, at a porosity of 0.2, the thermal conductivity and thermal diffusivity of the rocks from Merapi volcano are ~0.4 $\text{W}\cdot\text{m}^{-1}\cdot\text{K}^{-1}$ and ~0.2 $\text{mm}^2\cdot\text{s}^{-1}$ lower than respective values for the andesites from Mt. Ruapehu ([Figs. 3c and 4](#)).

4. Discussion

A decrease in thermal conductivity, thermal diffusivity, and specific heat capacity as porosity increases for the dry samples ([Figs. 3 and 4](#)) can be explained by the large difference in these thermal properties between rock-forming minerals and pore-filling air. A decrease in thermal properties as a function of increasing porosity has been observed previously for dry porous rocks (e.g., Robertson and Peck, 1974; Brigaud and Vasseur, 1989; Clauser and Huenges, 1995; Popov et al., 2003; Pimienta et al., 2014; Esteban et al., 2015; Mielke et al., 2015, 2017; Heap et al., 2019b; Harlé et al., 2019). The change in thermal properties following water saturation ([Fig. 5](#)) reflects the different thermal properties of pore-filling air and water (e.g., Nagaraju and Roy, 2014; Harlé et al., 2019): the thermal conductivity of air and water are ~0 and ~0.6 $\text{W}\cdot\text{m}^{-1}\cdot\text{K}^{-1}$, respectively. Finally, the reduction in thermal conductivity ([Fig. 3c](#)) and thermal diffusivity ([Fig. 4](#)) following hydrothermal alteration, for a given porosity, is interpreted here as the result of differences between the thermal properties of the primary and alteration minerals. Gypsum (one of the alteration minerals; [Table 1](#)), for example, has a very low thermal conductivity (Clauser and Huenges, 1995). The influence of hydrothermal alteration on the thermal properties of volcanic rock will also depend on whether the alteration increases or decreases porosity. For example, the alteration of ash tuff from the Tauhara geothermal field decreased porosity, resulting in an increase in thermal conductivity (Mielke et al., 2015).

Table 2

Connected porosity, bulk sample density, thermal conductivity, thermal diffusivity, and specific heat capacity of the dry volcanic rocks measured for this study. Asterisk indicates that the sample contains cristobalite (see [Heap and Kennedy, 2016](#); [Heap et al., 2019a](#)). The five blocks from Merapi volcano are labelled M-U ("unaltered"), M-SA1 and M-SA2 ("slightly altered"), and M-HA1 and M-AH2 ("highly altered") (as in [Heap et al., 2019a](#)). Quoted values of thermal conductivity and thermal diffusivity are the average of four measurements. The specific heat capacity was calculated by dividing the specific heat per unit volume, given by the Hot Disk device (using the average of the four measurements), by the bulk sample density. The standard deviations provided relate to measurement precision (calculated using the four measurements). The standard uncertainty for values of thermal conductivity and thermal diffusivity using the transient hot-strip method has been determined to be 2.6 and 11%, respectively ([Hammerschmidt and Sabuga, 2000](#)).

Volcano	Sample number	Bulk sample density, ρ_b (kg·m ⁻³)	Connected porosity	Thermal conductivity, λ (W·m ⁻¹ ·K ⁻¹)	Thermal diffusivity, D (mm ² ·s ⁻¹)	Specific heat capacity, C_p (kJ·kg ⁻¹ ·K ⁻¹)
Ruapehu	R1-1*	2760	0.021	1.54 ± 0.018	0.70 ± 0.020	0.80 ± 0.032
Ruapehu	R1-2*	2710	0.040	1.62 ± 0.016	0.77 ± 0.018	0.78 ± 0.010
Ruapehu	R2-1*	2714	0.024	1.47 ± 0.064	0.77 ± 0.074	0.72 ± 0.100
Ruapehu	R2-2*	2686	0.036	1.46 ± 0.051	0.75 ± 0.009	0.73 ± 0.016
Ruapehu	R3-1*	2706	0.042	1.53 ± 0.007	0.76 ± 0.035	0.74 ± 0.037
Ruapehu	R3-2*	2692	0.047	1.51 ± 0.050	0.72 ± 0.054	0.79 ± 0.085
Ruapehu	R4-1*	2669	0.038	1.45 ± 0.030	0.70 ± 0.033	0.77 ± 0.053
Ruapehu	R4-2*	2681	0.036	1.51 ± 0.005	0.72 ± 0.007	0.78 ± 0.005
Ruapehu	R5-1	2709	0.024	1.48 ± 0.016	0.71 ± 0.018	0.77 ± 0.028
Ruapehu	R5-2	2704	0.027	1.46 ± 0.031	0.68 ± 0.012	0.79 ± 0.003
Ruapehu	R6-1	2635	0.048	1.39 ± 0.011	0.83 ± 0.056	0.64 ± 0.039
Ruapehu	R6-2	2663	0.042	1.41 ± 0.002	0.67 ± 0.004	0.80 ± 0.004
Ruapehu	R7-1	2260	0.184	1.06 ± 0.010	0.65 ± 0.038	0.73 ± 0.049
Ruapehu	R7-2	2227	0.205	1.00 ± 0.047	0.58 ± 0.055	0.79 ± 0.112
Ruapehu	R8-1	2500	0.098	1.26 ± 0.013	0.70 ± 0.037	0.72 ± 0.045
Ruapehu	R8-2	2455	0.118	1.22 ± 0.058	0.65 ± 0.054	0.77 ± 0.100
Ruapehu	R9-1	2361	0.153	1.17 ± 0.048	0.66 ± 0.081	0.76 ± 0.057
Ruapehu	R9-2	2389	0.140	1.23 ± 0.051	0.71 ± 0.058	0.74 ± 0.080
Ruapehu	R10-1	2372	0.149	1.14 ± 0.043	0.65 ± 0.016	0.73 ± 0.046
Ruapehu	R10-2	2322	0.167	1.08 ± 0.092	0.72 ± 0.094	0.65 ± 0.030
Ruapehu	R11-1	2417	0.129	1.21 ± 0.045	0.59 ± 0.005	0.86 ± 0.039
Ruapehu	R11-2	2361	0.151	1.13 ± 0.052	0.60 ± 0.063	0.80 ± 0.048
Ruapehu	R12-1	2209	0.204	1.01 ± 0.046	0.61 ± 0.029	0.75 ± 0.002
Ruapehu	R12-2	2286	0.182	1.09 ± 0.018	0.62 ± 0.051	0.78 ± 0.051
Ruapehu	R13-1	1924	0.308	0.81 ± 0.004	0.64 ± 0.029	0.66 ± 0.033
Ruapehu	R14-1	1886	0.320	0.84 ± 0.003	0.75 ± 0.108	0.61 ± 0.104
Ruapehu	R14-2	1834	0.345	0.81 ± 0.041	0.52 ± 0.050	0.85 ± 0.046
Ruapehu	R15-1	1817	0.348	0.81 ± 0.060	0.59 ± 0.019	0.76 ± 0.053
Ruapehu	R15-2	1866	0.333	0.79 ± 0.052	0.53 ± 0.065	0.81 ± 0.072
Ruapehu	R16-1	1725	0.382	0.73 ± 0.044	0.63 ± 0.092	0.68 ± 0.138
Ruapehu	R17-1	1068	0.602	0.43 ± 0.026	0.51 ± 0.044	0.79 ± 0.020
Ruapehu	R17-2	999	0.628	0.38 ± 0.027	0.55 ± 0.082	0.71 ± 0.155
Merapi	MU* 5B4	2578	0.080	1.43 ± 0.022	0.70 ± 0.038	0.79 ± 0.031
Merapi	MU* 5B5	2564	0.084	1.37 ± 0.033	0.73 ± 0.031	0.74 ± 0.023
Merapi	MU* 5B8	2586	0.077	1.48 ± 0.025	0.73 ± 0.041	0.79 ± 0.037
Merapi	MSA2 2B4	2490	0.079	1.20 ± 0.015	0.57 ± 0.022	0.86 ± 0.041
Merapi	MSA2 2B6	2493	0.080	1.23 ± 0.052	0.57 ± 0.027	0.87 ± 0.019
Merapi	MSA2 2B8	2494	0.083	1.28 ± 0.015	0.53 ± 0.021	0.98 ± 0.030
Merapi	MHA1 4B4	2293	0.154	1.07 ± 0.068	0.51 ± 0.030	0.91 ± 0.041
Merapi	MHA1 4B5	2207	0.182	0.90 ± 0.059	0.51 ± 0.028	0.81 ± 0.014
Merapi	MHA1 4B6	2251	0.144	1.07 ± 0.049	0.53 ± 0.011	0.91 ± 0.059
Merapi	MHA1 4B7	2266	0.155	1.04 ± 0.013	0.52 ± 0.022	0.88 ± 0.041
Merapi	MHA1 4B8	2233	0.160	0.97 ± 0.079	0.54 ± 0.027	0.81 ± 0.056
Merapi	MHA1 4B9	2254	0.162	0.97 ± 0.008	0.66 ± 0.210	0.73 ± 0.227
Merapi	MHA1 4B10	2189	0.182	0.94 ± 0.004	0.43 ± 0.001	0.99 ± 0.003
Merapi	MHA2* 3B4	2061	0.215	0.78 ± 0.076	0.60 ± 0.094	0.66 ± 0.185
Merapi	MHA2* 3B5	2013	0.233	0.80 ± 0.037	0.51 ± 0.087	0.79 ± 0.103
Merapi	MHA2* 3B6	2036	0.220	0.86 ± 0.066	0.51 ± 0.043	0.82 ± 0.019
Merapi	MHA2* 3B7	2108	0.188	0.86 ± 0.060	0.50 ± 0.027	0.83 ± 0.021
Merapi	MHA2* 3B8	2173	0.163	0.88 ± 0.008	0.55 ± 0.045	0.75 ± 0.063
Merapi	MHA2* 3B9	1990	0.242	0.79 ± 0.049	0.46 ± 0.004	0.86 ± 0.046
Merapi	MHA2*3B10	1938	0.263	0.79 ± 0.011	0.47 ± 0.042	0.88 ± 0.067
Merapi	MHA2*3B11	2166	0.168	0.85 ± 0.028	0.45 ± 0.093	0.93 ± 0.195
Merapi	MSA1 1A4	2116	0.231	0.75 ± 0.061	0.45 ± 0.062	0.80 ± 0.107
Merapi	MSA1 1A6	2102	0.236	0.76 ± 0.052	0.51 ± 0.018	0.70 ± 0.071
Merapi	MSA1 1A8	2033	0.262	0.76 ± 0.038	0.55 ± 0.105	0.70 ± 0.109
Merapi	MSA1 1A10	2048	0.256	0.75 ± 0.049	0.47 ± 0.052	0.78 ± 0.062

4.1. Theoretical predictions

The effective thermal conductivity, $\lambda(\phi)$, can be determined using the Maxwell equation:

$$\frac{\lambda(\phi)}{\lambda_0} = \frac{(1-\phi)(1-m) + m\beta\phi}{(1-\phi)(1-m) + \beta\phi}, \quad (1)$$

where ϕ is the total porosity, $m = \lambda_f/\lambda_0$ (where λ_0 and λ_f are the thermal conductivities of the rock groundmass and the fluid within the pore space, respectively), and, for spherical pores, $\beta = 3(1-m)/(2+m)$ ([Zimmerman, 1989](#)). The Maxwell model assumes no interaction between the spherical pores. To determine thermal conductivity as a function of porosity for our dry and water-saturated samples, we assume that the thermal conductivity of air and water are 0 and 0.6 W·m⁻¹·K⁻¹, respectively (e.g., [Nagaraju and Roy, 2014](#); [Vosteen](#)

Table 3

Average connected porosity, bulk sample density (of the water-saturated samples), thermal conductivity, thermal diffusivity, and specific heat capacity for the water-saturated andesites from Mt. Ruapehu. Asterisk indicates that the sample contains cristobalite (see Heap and Kennedy, 2016). Quoted values of thermal conductivity and thermal diffusivity are the average of four measurements. The specific heat capacity was calculated by dividing the specific heat per unit volume, given by the Hot Disk device (using the average of the four measurements), by the bulk sample density. The standard deviations provided relate to measurement precision (calculated using the four measurements). The standard uncertainty for values of thermal conductivity and thermal diffusivity using the transient hot-strip method has been determined to be 2.6 and 11%, respectively (Hammerschmidt and Sabuga, 2000).

Volcano	Sample number	Average bulk sample density, ρ_b (kg·m ⁻³)	Average connected porosity	Thermal conductivity, λ (W·m ⁻¹ ·K ⁻¹)	Thermal diffusivity, D (mm ² ·s ⁻¹)	Specific heat capacity, C_p (kJ·kg ⁻¹ ·K ⁻¹)
Ruapehu	R1*	2765	0.030	1.95 ± 0.068	0.85 ± 0.113	0.84 ± 0.107
Ruapehu	R2*	2730	0.030	1.67 ± 0.021	0.75 ± 0.027	0.82 ± 0.029
Ruapehu	R3*	2744	0.044	1.92 ± 0.046	0.78 ± 0.094	0.90 ± 0.091
Ruapehu	R4*	2712	0.037	1.67 ± 0.021	0.75 ± 0.027	0.83 ± 0.029
Ruapehu	R5	2732	0.026	1.52 ± 0.056	0.63 ± 0.032	0.88 ± 0.027
Ruapehu	R6	2694	0.045	1.51 ± 0.063	0.64 ± 0.062	0.88 ± 0.051
Ruapehu	R7	2438	0.195	1.37 ± 0.030	0.54 ± 0.045	1.04 ± 0.066
Ruapehu	R8	2586	0.108	1.47 ± 0.021	0.60 ± 0.061	0.96 ± 0.105
Ruapehu	R9	2522	0.147	1.42 ± 0.042	0.57 ± 0.053	0.99 ± 0.074
Ruapehu	R10	2505	0.158	1.42 ± 0.034	0.60 ± 0.033	0.96 ± 0.049
Ruapehu	R11	2530	0.140	1.42 ± 0.040	0.61 ± 0.012	0.92 ± 0.021
Ruapehu	R12	2440	0.193	1.35 ± 0.024	0.55 ± 0.008	1.01 ± 0.020
Ruapehu	R14	2192	0.333	1.27 ± 0.025	0.49 ± 0.023	1.20 ± 0.080
Ruapehu	R15	2182	0.341	1.31 ± 0.061	—	—
Ruapehu	R17	1649	0.615	0.90 ± 0.024	0.27 ± 0.010	2.02 ± 0.021

and Schellschmidt, 2003). Eq. (1) well describes the data for the dry (solid black line; Fig. 3c) and wet (dashed blue line; Fig. 3c) andesites from Mt. Ruapehu, providing a value for λ_0 of 1.50 W·m⁻¹·K⁻¹. We also plot data for variably porous dry basalt from Robertson and Peck (1974) in Fig. 3c (grey triangles), which are also well described by Eq. (1) (see also Horai, 1991). However, although the low-porosity rocks (porosity <0.1) from Merapi volcano, those characterised by low levels of hydrothermal alteration, follow the trend delineated by a λ_0 of 1.50 W·m⁻¹·K⁻¹, the more altered rocks, containing a higher porosity (from ~0.15 to ~0.25), fall consistently below the trend (Fig. 3c). This discrepancy can be explained by a change in λ_0 as a result of the change in the mineral assemblage due to hydrothermal alteration. Our data show that the minimum possible value of λ_0 for the altered rocks from Merapi volcano, using Eq. (1), is 1.10 W·m⁻¹·K⁻¹ (dotted green line; Fig. 3c).

The effective thermal diffusivity $D(\phi)$ can be obtained using (e.g., Connor et al., 1997):

$$D(\phi) = \frac{\lambda(\phi)}{\rho_s C_p(1-\phi) + \rho_f C_{p,f}\phi} \quad (2)$$

where ρ_s and ρ_f are the matrix and pore fluid densities, respectively, and C_p and $C_{p,f}$ are the matrix and pore fluid specific heat capacity, respectively. Based on Eq. (2), the effective specific heat capacity $C_p(\phi)$ can be derived as:

$$C_p(\phi) = \frac{\rho_s C_p(1-\phi) + \rho_f C_{p,f}\phi}{\rho_b} \quad (3)$$

To model the thermal diffusivity and specific heat capacity data for the andesites from Mt. Ruapehu, we use $\rho_s = 2750$ kg·m⁻³ and $C_p = 0.750$ kJ·kg⁻¹·K⁻¹ (values selected based on our laboratory measurements for the Mt. Ruapehu samples; Table 2), $\rho_f = 1.275$ kg·m⁻³ and $C_{p,f} = 1.007$ kJ·kg⁻¹·K⁻¹ for air, and $\rho_f = 1000$ kg·m⁻³ and $C_{p,f} = 4.182$ kJ·kg⁻¹·K⁻¹ for water. We find that Eq. (2) can well describe the dry (solid black line in Fig. 4) and water-saturated (dashed blue line in Fig. 4) thermal diffusivity data for the Mt. Ruapehu andesites. We also find that Eq. (3) well describes the dry (solid black line in Fig. 3b) and water-saturated (dashed black line in Fig. 3b) specific heat capacity data. We also provide theoretical curves, using Eqs. (1)–(3), for the wet/dry ratios for the specific heat capacity, thermal conductivity, and thermal diffusivity data (solid black lines in Fig. 5). We find

that the theoretical predictions for the wet/dry ratios also well describe our experimental data (Fig. 5).

The fact that Eqs. (1)–(3) can accurately describe the thermal conductivity, thermal diffusivity, and specific heat capacity of the andesites from Ruapehu, despite their microstructural differences (e.g., differences in pore size, pore shape, microcrack density; Fig. 1), highlights that porosity exerts a first order control on the thermal properties of porous andesites.

4.2. Case studies: heat loss from a dyke and conduit

It is important to assess whether the measured changes to thermal conductivity, thermal diffusivity, and specific heat capacity as a function of porosity and alteration (Figs. 3 and 4; Tables 2 and 3) are sufficient to influence volcanic/geothermal processes. To do so, we model the migration of the 700 °C isotherm with respect to the boundary of a dyke and a conduit by solving the heat equation in 1D for two different coordinate systems: (1) Cartesian (analogous to dyke geometry) and (2) cylindrical (analogous to conduit geometry) coordinates. We explore a scenario in which the magma in the dyke or conduit is stagnant and loses heat to the host-rock through conduction, leading to wholescale cooling of the system. Fick's second law for heat transfer by conduction is given by (Crank, 1979):

$$\frac{\partial T}{\partial t} = \nabla \cdot (D(\phi) \nabla T), \quad (4)$$

where t is the time since the onset of heat transfer, T is the temperature, and $D(\phi)$ is the effective thermal diffusivity. In 1D, the right-hand side of Eq. (4) becomes (Crank, 1979, pages 56 and 69):

$$\frac{\partial}{\partial x} \left(D(\phi) \frac{\partial T}{\partial x} \right); \quad \text{cartesian coordinates – dyke geometry}$$

$$\frac{1}{r} \frac{\partial}{\partial r} \left(r D(\phi) \frac{\partial T}{\partial r} \right); \quad \text{cylindrical coordinates – conduit geometry}$$

In Cartesian coordinates, x represents for the distance from the dyke centre (assuming an axisymmetric dyke) and, in cylindrical coordinates, r represents for the radial distance from the conduit centre. In both cases we have the same initial conditions at $t = 0$ that $T = T_m$ for $x \leq L$ and $r \leq R$, and $T = T_r$ for $x > L$ and $r > R$, where T_m and T_r are the initial temperature of the magma and the host-rock, respectively, and L and R are the dyke half-width and conduit radius, respectively. T_m is only applied

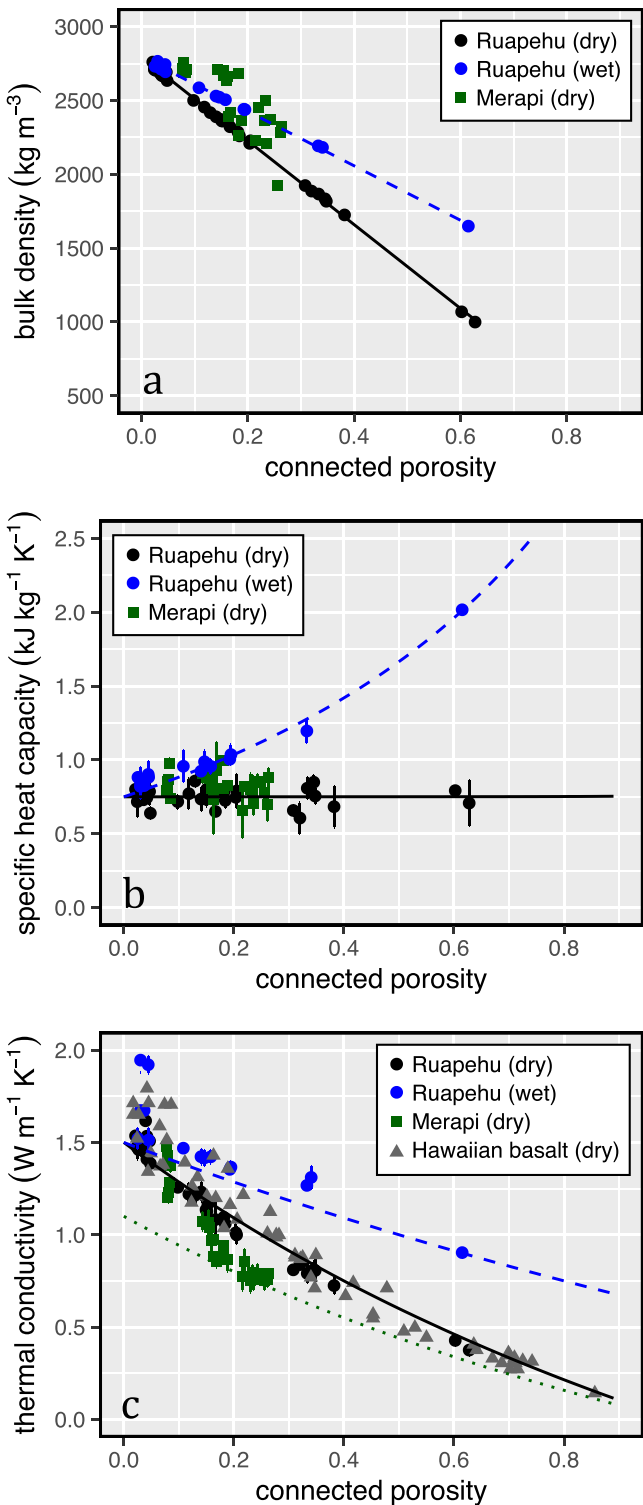


Fig. 3. (a) Bulk sample density, (b) specific heat capacity, and (c) thermal conductivity as a function of connected porosity for the andesites from Mt. Ruapehu and the altered basaltic-andesites from Merapi volcano (see Tables 2 and 3). Solid, dashed, and dotted lines correspond to theoretical curves (see text for details). Blue circles – Mt. Ruapehu (wet); black circles – Mt. Ruapehu (dry); green squares – Merapi volcano (dry); grey triangles – Hawaiian basalt (data from Robertson and Peck, 1974). The standard uncertainty for values of thermal conductivity and thermal diffusivity using the transient hot-strip method has been determined to be 2.6 and 11%, respectively (Hammerschmidt and Sabuga, 2000).

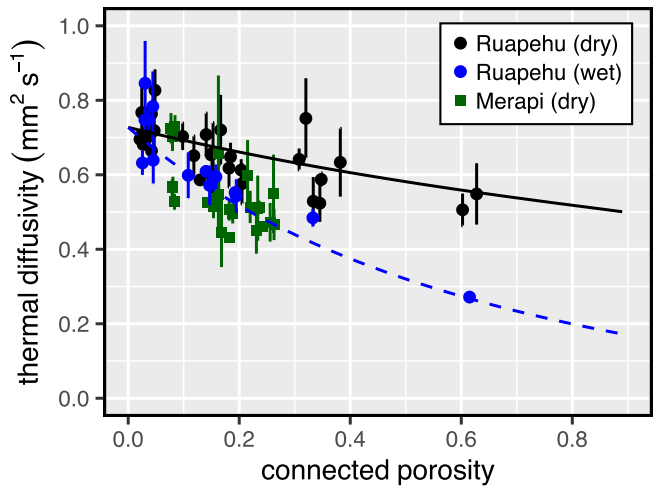


Fig. 4. Thermal diffusivity as a function of connected porosity for the andesites from Mt. Ruapehu and the altered basaltic-andesites from Merapi volcano (see Tables 2 and 3). Solid and dashed lines correspond to theoretical curves (see text for details). Blue circles – Mt. Ruapehu (wet); black circles – Mt. Ruapehu (dry); green squares – Merapi volcano (dry). The standard uncertainty for values of thermal diffusivity using the transient hot-strip method has been determined to be 11% (Hammerschmidt and Sabuga, 2000).

at the start (i.e. $t = 0$) and the magma cools down by conducting heat to the host-rock. We take a range of T_m from 800 to 1200 °C and $T_r = 50$ °C. We consider a pore-free magma and explore the influence of the porosity of the host-rock on the migration of the isotherm (i.e. the cooling of the system). We scale the effect of porosity by decomposing the bulk specific heat capacity using Eq. (3), and by using the Maxwell equation for the bulk thermal conductivity (Eq. (1)). The use of these theoretical relationships is supported by their accurate description of our experimental data (Fig. 3a and c) (the maximum and minimum difference between the data and the value predicted by the model are 0.205 and $-0.089 \text{ W} \cdot \text{m}^{-1} \cdot \text{K}^{-1}$ and 0.107 and $-0.144 \text{ kJ} \cdot \text{kg}^{-1} \cdot \text{K}^{-1}$ for thermal conductivity and specific heat capacity, respectively). We also use our experimental data to constrain the matrix properties of the host-rock, such that $\rho = 2750 \text{ kg} \cdot \text{m}^{-3}$, $\lambda_0 = 1.50 \pm 1 \text{ W} \cdot \text{m}^{-1} \cdot \text{K}^{-1}$, and $C_p = 0.750 \pm 0.010 \text{ kJ} \cdot \text{kg}^{-1} \cdot \text{K}^{-1}$. As above, we use $\rho_f = 1.275 \text{ kg} \cdot \text{m}^{-3}$ and $C_{p,f} = 1.007 \text{ kJ} \cdot \text{kg}^{-1} \cdot \text{K}^{-1}$ for air. Our modelling therefore uses data collected at ambient laboratory pressure and temperature (see our “Data limitations” section below). In our simulations of heat transfer, both dyke and conduit centres are insulated (Neumann boundary condition of 0) such that $\partial T/\partial x = \partial T/\partial r = 0$ for all t . The far-field temperature in the host-rock is kept constant at T_r . We take a typical dyke half-width and conduit radius of $L = R = 25 \text{ m}$. We explicitly acknowledge that our approach does not account for the advection or convection of heat (in the magma and in the host-rock). It is also assumed that no heat is generated. With these conditions, we solve Eq. (4) numerically using a backward-time, centred-space finite difference scheme. The model setup is presented in Fig. 6.

The resulting migration of the 700 °C isotherm as a function of time are shown in Fig. 7a (dyke geometry) and Fig. 8a (conduit geometry), for air-filled pores, initial magma temperatures, T_m , of 800, 1000, and 1200 °C, and host-rock porosities, ϕ , of 0, 0.3, and 0.6. Figs. 7a and 8a show that there is a large influence of initial magma temperature on the migration of the isotherm. For example, after 50 days, and for a porosity of 0.3, the isotherm moves 2.7, 1.1, and 0.2 m from the boundary of the dyke at initial magma temperatures of 800, 1000, and 1200 °C, respectively (Fig. 7a). The isotherm moves 2.9, 1.2, and 0.4 m from the boundary of the conduit (i.e. inside the conduit) after 50 days (assuming a porosity of 0.3) at initial magma temperatures of 800, 1000, and 1200 °C, respectively (Fig. 8a). Host-rock porosity also influences the

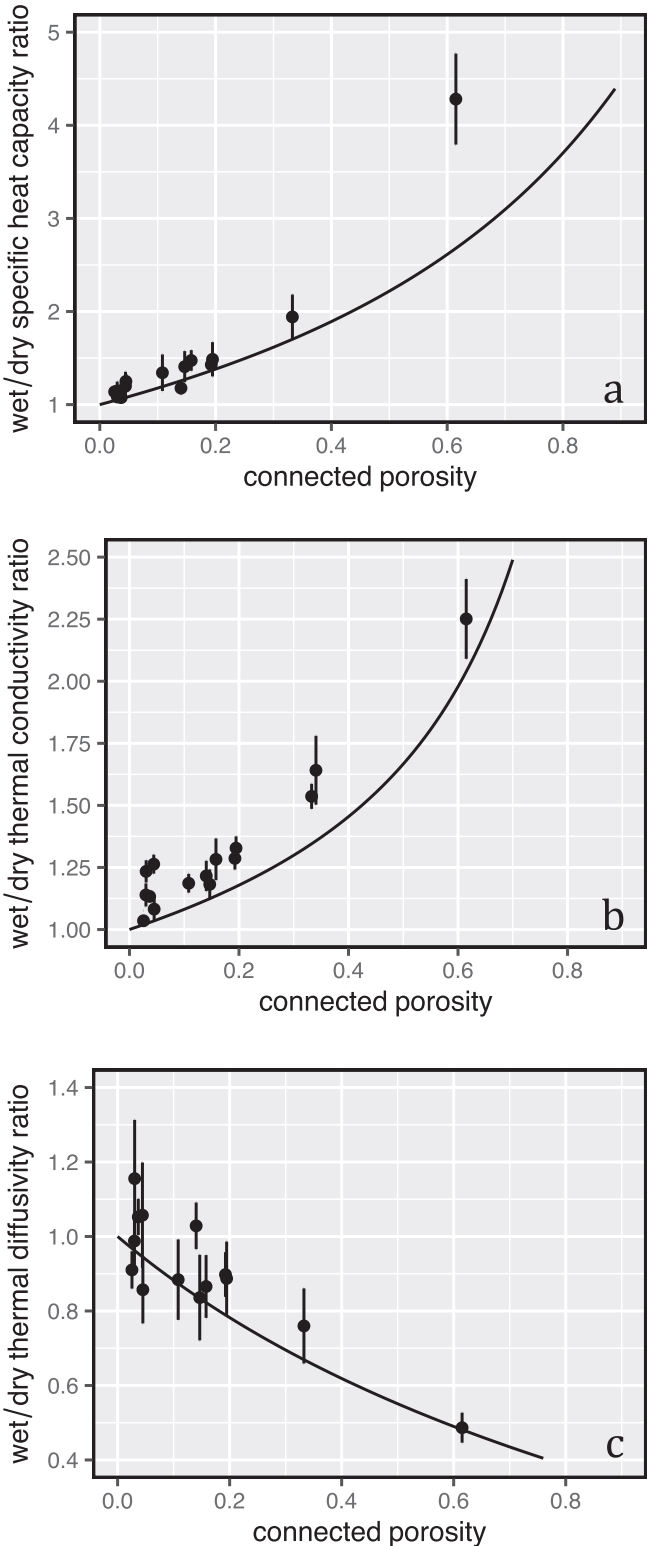


Fig. 5. The ratio of wet-to-dry (a) thermal conductivity, (b) thermal diffusivity, and (c) specific heat capacity as a function of connected porosity for the samples from Mt. Ruapehu. Solid lines correspond to theoretical curves (see text for details).

migration of the isotherm (Figs. 7a and 8a). Following 50 days, for an initial magma temperature of 1200 °C, the isotherm moves from the dyke and conduit boundary by 0.4, 0.2, and 0.1 m and 0.6, 0.4, and 0.2 m for host-rock porosities of 0, 0.3, and 0.6, respectively (Figs. 7a and 8a).

We additionally approximate the effect of host-rock hydrothermal alteration on the cooling of a dyke and conduit. To do so, the matrix thermal conductivity, λ_0 , was changed from 1.50 ± 1 to $1.10 \pm 1 \text{ W} \cdot \text{m}^{-1} \cdot \text{K}^{-1}$, as guided by our experimental data (Fig. 3c). All other parameters remained unchanged. Figs. 7b and 8b show the results (for a host-rock porosity of 0.1, air-filled pores, and an initial magma temperature of 1000 °C) for the dyke and conduit geometries, respectively. It can be seen that host-rock hydrothermal alteration influences the migration of the isotherm (Figs. 7b and 8b). For example, after 50 days, the 700 °C isotherm moves from the dyke and conduit boundary by 1.2 and 1.0 m and 1.3 and 1.1 m for $\lambda_0 = 1.50$ (i.e. unaltered) and $\lambda_0 = 1.10 \text{ W} \cdot \text{m}^{-1} \cdot \text{K}^{-1}$ (i.e. altered), respectively (Figs. 7b and 8b).

4.3. Data limitations

First, as outlined in our methods section, the standard uncertainty of our thermal conductivity and thermal diffusivity measurements is 2.6 and 11%, respectively (Hammerschmidt and Sabuga, 2000). Data collected using the method used suffers from contact losses and ballistic radiative transfer gains (Hofmeister, 2019). Second, our measurements were performed at ambient pressure and temperature. For example, an increase in pressure (i.e. depth) will close microcracks (e.g., Vinciguerra et al., 2005; Nara et al., 2011; Zhu et al., 2016), abundant in these materials (Fig. 1). A reduction in porosity, due to the closure of microcracks, will likely increase thermal conductivity, thermal diffusivity, and specific heat capacity (Figs. 3 and 4; Eq. (1)). However, we note that microcracks typically only represent a very small proportion of the porosity within a sample due to their very low aspect ratio (e.g., Kranz, 1983). Therefore, our measurements, performed at room pressure, will likely slightly underestimate the thermal properties of volcanic rock at depth. An increase in temperature has been shown to influence the thermal properties of rocks and rock-forming minerals (e.g., Guéguen and Palciauskas, 1994; Nabelek et al., 2010; Guo et al., 2017; Vosteen and Schellschmidt, 2003; Harlé et al., 2019), including volcanic rocks (e.g., Bates et al., 1970; Horai et al., 1970; Petrunin et al., 1971; Fujii and Osako, 1973; Büttner et al., 1998; Romine et al., 2012; Hofmeister, 2019). Compiled thermal diffusivity data for volcanic materials show that the largest differences in thermal diffusivity occur at temperatures below ~300 °C (Fig. 9). For example, Romine et al. (2012) found that the thermal diffusivity of rhyolite decreased from ~0.65 to ~0.55 $\text{mm}^2 \cdot \text{s}^{-1}$ as temperature was increased from ~20 to ~430 °C, but remained constant from ~430 to ~1300 °C. We also note that the differences as a result of porosity variation (data from this study) are as large as the variation in thermal diffusivity as temperature is increased from ~20 to ~1300 °C (Fig. 9). Therefore, although our measurements were performed at room temperature and likely overestimate the thermal diffusivity of volcanic rock at high-temperature, relatively small changes in thermal diffusivity between ~300 and ~1300 °C (Fig. 9) provides some support for the assumption of a constant thermal diffusivity in our modelling. It is clear, however, that thermal property measurements at high temperature are now required for a range of variably porous volcanic rocks. An increase in temperature can also generate thermal microcracks that will also serve to decrease thermal conductivity and thermal diffusivity (Kant et al., 2017). However, although rocks such as granites are well known to suffer thermal microcracking when exposed to high-temperature (e.g., Homand-Etienne and Houpert, 1989; David et al., 1999; Chaki et al., 2008; Griffiths et al., 2018), the microstructure of some volcanic rocks is unaffected (e.g., Vinciguerra et al., 2005; Heap et al., 2018; Coats et al., 2018; Eggertsson et al., 2018). Measuring the thermal properties for a range of volcanic rocks at a range of pressures and temperatures offers an exciting avenue for future research.

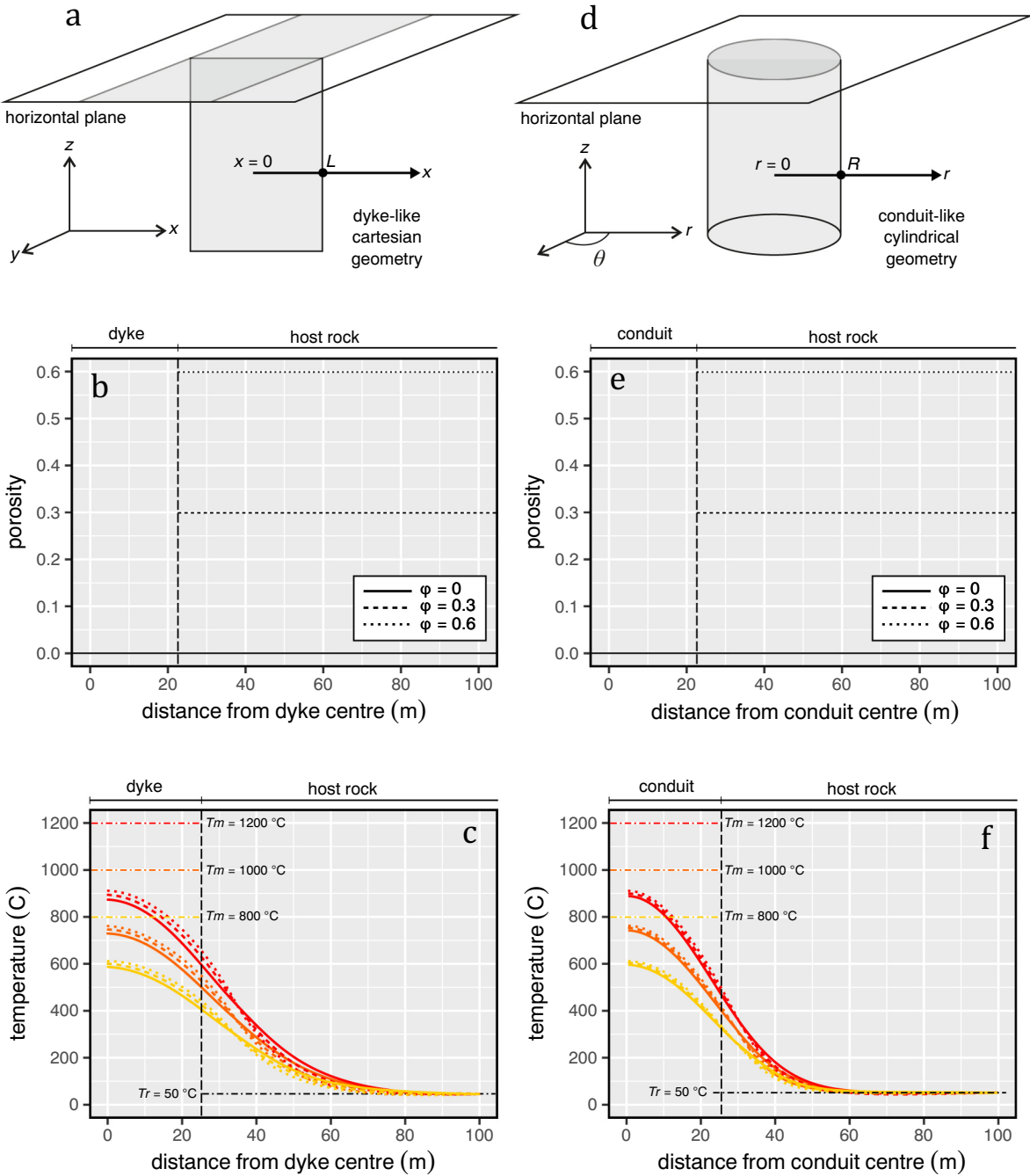


Fig. 6. Model set up and example results using the thermal properties for the host-rock (or edifice) constrained herein. We present two suites of simplified conduction model, for heat transfer from a dyke (a-c) or from a cylindrical conduit (d-f). Panels (a) and (d) show the general coordinate system (we do not introduce the coordinate directions y , z , or θ in the text because these are implicit in the derivation for each geometry). In panels (b-c) and (e-f), the vertical dashed grey line represents the dyke margin (b-c; $x = L$) or the conduit margin (e-f; $r = R$). In panels (b) and (e) we show the distribution of the porosity across the domain, which is imposed throughout the simulations, where the magma is always at zero porosity, and the country rock has a porosity of 0, 0.3, or 0.6 (each solution type is delineated by line style). In panels (c) and (f) we show an example suite of solutions for the evolution of temperature across the domain for each geometry, and also mark the initial magma temperature T_m (colour delineates the three magma temperatures investigated), and the country rock temperature $T_r = 50$ °C. The thermal property determinations at low temperature are most applicable to the evolution of temperature in the host-rock far field, relevant to the geothermal system, but we note that these simulations show that the thermal evolution in this host-rock domain depends on the thermal pathway taken by the magma, as well as the geometry of the system.

4.4. Implications

The thermal property data provided herein (Tables 2 and 3) can be used for a wide range of modelling endeavours. We note that, because Eqs. (1)–(3) are suitable approximations for the data collected for this study (Figs. 3 and 4), the thermal property structure of a volcano or volcanic environment could be estimated using geophysical methods that

provide images of the subsurface in terms of density or porosity, such as muon tomography (Tanaka et al., 2010; Marteau et al., 2012; Lesparre et al., 2012; Rosas-Carbajal et al., 2017). Therefore, if the saturation state of the edifice is known, or can be approximated, Eqs. (1)–(3) could be used to estimate the thermal property structure of a volcano that could, in turn, be employed to model heat flow within a volcanic edifice.

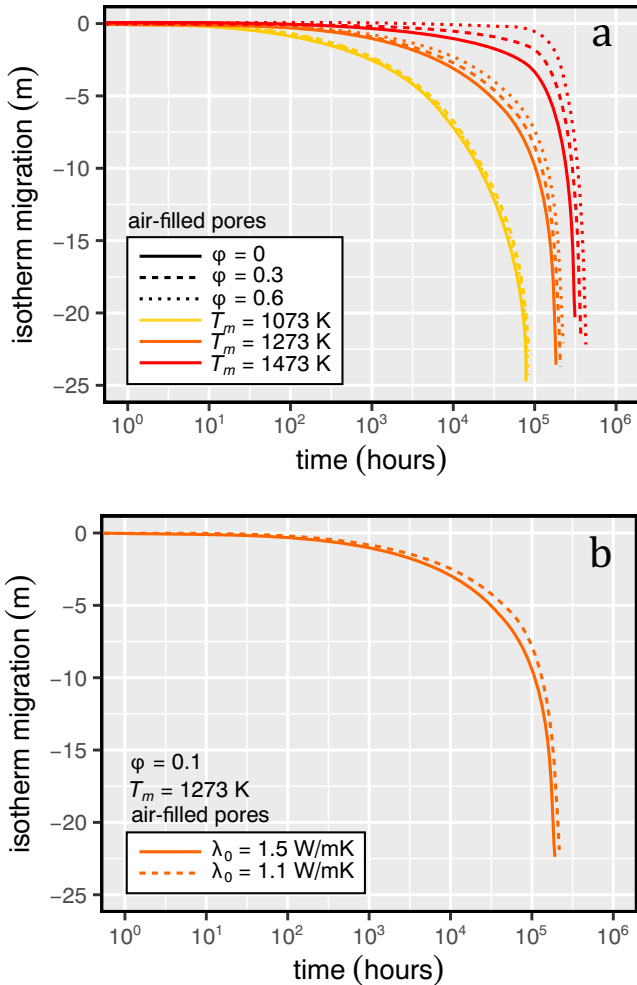


Fig. 7. (a) The migration of the 700 °C isotherm within a dyke (dyke half-width = 25 m) as a function of time for an unaltered host-rock with air-filled pores. Modelled curves are provided for different initial magma temperatures (800, 1000, and 1200 °C) and different host-rock porosities (0, 0.3, and 0.6). (b) The migration of the 700 °C isotherm within a dyke as a function of time for host-rocks with different thermal conductivities chosen to represent unaltered host-rock ($\lambda_0 = 1.50 \text{ W} \cdot \text{m}^{-1} \cdot \text{K}^{-1}$) and hydrothermally altered host-rock ($\lambda_0 = 1.10 \text{ W} \cdot \text{m}^{-1} \cdot \text{K}^{-1}$). Both curves are for an initial magma temperature of 1000 °C and a host-rock porosity of 0.1.

Our modelling (Figs. 7 and 8) also highlights that hydrothermal alteration slows the cooling of a dyke and conduit. Therefore, progressive hydrothermal alteration of an edifice or lava dome could keep a conduit-dwelling magma or the core of a dome hotter for longer, respectively. Indeed, the maintenance of these elevated temperatures may promote further alteration within the edifice or dome. Hydrothermal alteration of volcanic rocks can result in decreases to rock strength (e.g., Pola et al., 2012; Wyering et al., 2014; Frolova et al., 2014; Heap et al., 2015; Farquharson et al., 2019; Mordensky et al., 2019). Thus, as edifices remain under temperature and fluid conditions amenable to alteration, their structure may become progressively unstable and more prone to mass-wasting events (e.g., López and Williams, 1993; Reid et al., 2001; Finn et al., 2001; Ball et al., 2013, 2015). The volume of edifice material available to such events will be, in part, defined by the extent of alteration, where planes of failure are more likely to be found in areas with extensive alteration. An increase in the spatial distribution and/or intensity of alteration will also hasten permeability reductions as a result of pore- and crack-filling alteration, a process linked to erratic explosive behaviour (Heap et al., 2019a). We further note that recent discrete element modelling has shown that the volume of material in a dome collapse is larger when the ductile core of the dome is smaller,

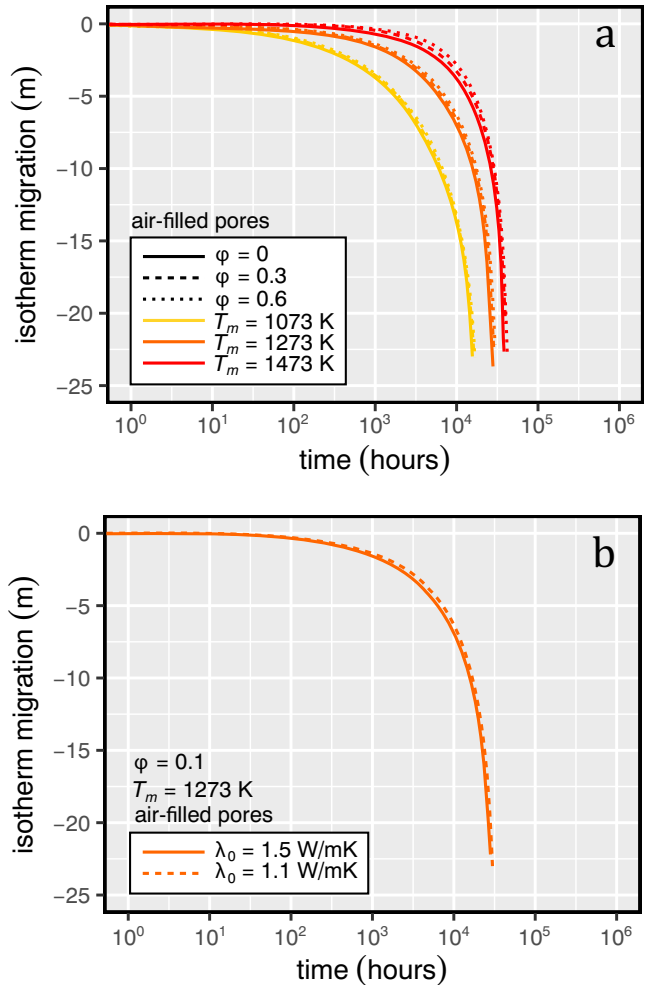


Fig. 8. (a) The migration of the 700 °C isotherm within a conduit (conduit radius = 25 m) as a function of time for a host-rock with air-filled pores. Modelled curves are provided for different initial magma temperatures (800, 1000, and 1200 °C) and different host-rock porosities (0, 0.3, and 0.6). (b) The migration of the 700 °C isotherm within a conduit as a function of time for host-rocks with different thermal conductivities chosen to represent unaltered host-rock ($\lambda_0 = 1.50 \text{ W} \cdot \text{m}^{-1} \cdot \text{K}^{-1}$) and hydrothermally altered host-rock ($\lambda_0 = 1.10 \text{ W} \cdot \text{m}^{-1} \cdot \text{K}^{-1}$). Both curves are for an initial magma temperature of 1000 °C and a host-rock porosity of 0.1.

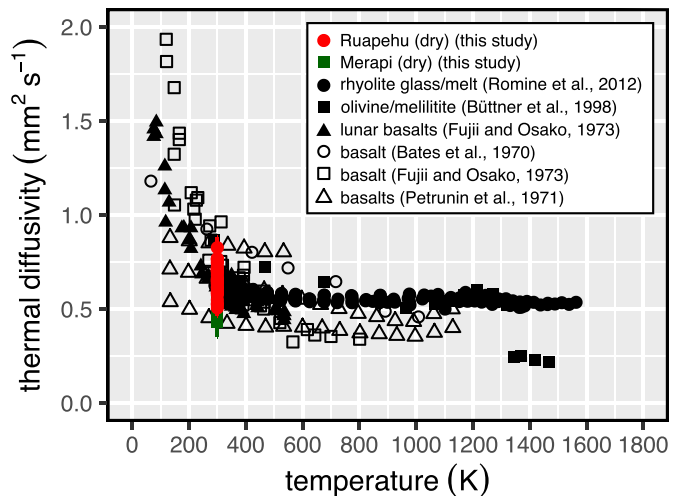


Fig. 9. Thermal diffusivity for volcanic materials as a function of temperature. Data from: this study, Romine et al. (2012), Büttner et al. (1998), Fujii and Osako (1973), Bates et al. (1970), and Petrunin et al. (1971).

as it controls the depth to which a shear plane can form (Harnett et al., 2018). Therefore, if the hydrothermal alteration of the talus rocks forming the outer shell of a lava dome can inhibit the cooling of the ductile dome core, hydrothermal alteration could limit the volume of material mobilised during the collapse of a lava dome. We consider it important, therefore, to monitor the extent and progression of hydrothermal alteration at active volcanoes using geophysical methods such as electrical tomography (e.g., Rosas-Carbajal et al., 2016; Byrdina et al., 2017; Soueid Ahmed et al., 2018; Ghorbani et al., 2018), gas monitoring (e.g., de Moor et al., 2019), or methods such as visible and infrared spectroscopy (Crowley and Zimbelman, 1997; John et al., 2008) and hyperspectral analysis (Kereszturi et al., 2018).

5. Conclusions

The thermal properties of volcanic rocks are sought-after parameters for numerous modelling endeavours. Here we present laboratory-measured values of thermal conductivity, thermal diffusivity, and specific heat capacity of variably porous andesites. Our data show that thermal conductivity, thermal diffusivity, and specific heat capacity of dry andesites all decrease as a function of increasing porosity. Relative to the dry state, saturation with water increases the thermal conductivity and specific heat capacity of the andesites, but decreases their thermal diffusivity. Additionally, our data show that hydrothermal alteration, specifically acid-sulphate alteration, increases the specific heat capacity and decreases the thermal conductivity and thermal diffusivity. We find that the measured experimental values agree well with theoretical predictions, suggesting that, despite the microstructural complexity of volcanic rocks, porosity is the principal parameter dictating their thermal properties. To understand whether the measured changes in thermal properties are sufficient to influence natural processes, we provide modelling that shows how the cooling of a dyke and conduit is slowed by a higher host-rock porosity and by increasing host-rock hydrothermal alteration. The values of thermal conductivity, thermal diffusivity, and specific heat capacity provided herein can help improve modelling designed to inform on volcanic and geothermal processes.

Declaration of competing interest

The authors declare that they have no known competing financial interests or personal relationships that could have appeared to influence the work reported in this paper.

Acknowledgements

This study received funding from Labex grant ANR-11-LABX-0050_G-EAU-THERMIE-PROFONDE and therefore benefited from state funding managed by the Agence National de la Recherche (ANR) as part of the "Investissements d'avenir" program. V.R.T. and F.M.D. acknowledge funding from the Swedish Research Council (Vetenskapsrådet). Special thanks to Harry Keys and Blake McDavid (previously at the New Zealand Department of Conservation), Ngati Tuwharetoa, Ngati Rangi, and Ruapehu Alpine Lifts for providing access and permission to sample at Ruapehu. We also thank Nadhirah Seraphine for logistical support and Hanik Humaida at the Balai Penyelidikan dan Pengembangan Teknologi Kebencanaan Geologi (BPPTKG, Yogyakarta) for rewarding discussions on Merapi volcano. We also thank Olivier Lengliné for valuable assistance. The constructive comments of Ingo Sonder and two anonymous reviewers helped improve the clarity of this manuscript.

Author contributions

M.J.H led the project and wrote the manuscript. A.R.L.K. and P.H. measured the dry and wet thermal properties, respectively. J.V. performed the modelling. M.J.H., B.K., V.R.T., and F.M.D. collected the

samples used in this study. All of the authors contributed to the interpretation of the data and the writing of the manuscript.

References

- Annen, C., 2017. Factors affecting the thickness of thermal aureoles. *Front. Earth Sci.* 5, 82.
- Annen, C., Pichavant, M., Bachmann, O., Burgisser, A., 2008. Conditions for the growth of a long-lived shallow crustal magma chamber below Mount Pelée volcano (Martinique, Lesser Antilles Arc). *Journal of Geophysical Research: Solid Earth* 113 (B7).
- Bagdassarov, N., Dingwell, D., 1994. Thermal properties of vesicular rhyolite. *J. Volcanol. Geotherm. Res.* 60 (2), 179–191.
- Ball, J.L., Calder, E.S., Hubbard, B.E., Bernstein, M.L., 2013. An assessment of hydrothermal alteration in the Santiaguito lava dome complex, Guatemala: implications for dome collapse hazards. *Bull. Volcanol.* 75 (1), 676.
- Ball, J.L., Stauffer, P.H., Calder, E.S., Valentine, G.A., 2015. The hydrothermal alteration of cooling lava domes. *Bull. Volcanol.* 77 (12), 102.
- Bates, J.L., McNeilly, C.E., Rasmussen, J.J., 1970. Properties of Molten Ceramics. Batelle Memorial Institute, Richland, Washington BNWL-SA-3529.
- Bauer, S.J., Handin, J., 1983. Thermal expansion and cracking of three confined water-saturated igneous rocks to 800 °C. *Rock Mech. Rock Eng.* 16 (3), 181–198.
- Bodvarsson, G.S., Pruess, K., Stefansson, V., Eliasson, E.T., 1984. The Krafla geothermal field, Iceland: 2. The natural state of the system. *Water Resour. Res.* 20 (11), 1531–1544.
- Brigaud, F., Vasseur, G., 1989. Mineralogy, porosity and fluid control on thermal conductivity of sedimentary rocks. *Geophys. J. Int.* 98 (3), 525–542.
- Bruce, P.M., Huppert, H.E., 1989. Thermal control of basaltic fissure eruptions. *Nature* 342 (6250), 665.
- Büttner, R., Zimanowski, B., Blumm, J., Hagemann, L., 1998. Thermal conductivity of a volcanic rock material (olivine-melilitite) in the temperature range between 288 and 1470 K. *J. Volcanol. Geotherm. Res.* 80 (3–4), 293–302.
- Byrdina, S., Friedel, S., Vandemeulebrouck, J., Budi-Santoso, A., Suryanto, W., Rizal, M.H., Winata, E., 2017. Geophysical image of the hydrothermal system of Merapi volcano. *J. Volcanol. Geotherm. Res.* 329, 30–40.
- Carrigan, C.R., 1984. Time and temperature dependent convection models of cooling reservoirs: application to volcanic sills. *Geophys. Res. Lett.* 11 (8), 693–696.
- Carrigan, C.R., Schubert, G., Eichelberger, J.C., 1992. Thermal and dynamical regimes of single-and two-phase magmatic flow in dikes. *Journal of Geophysical Research: Solid Earth* 97 (B12), 17377–17392.
- Chaki, S., Takarli, M., Agbodjan, W.P., 2008. Influence of thermal damage on physical properties of a granite rock: porosity, permeability and ultrasonic wave evolutions. *Constr. Build. Mater.* 22 (7), 1456–1461.
- Chiodini, G., Frondini, F., Cardellini, C., Granieri, D., Marini, L., Ventura, G., 2001. CO₂ degassing and energy release at Solfatara volcano, Campi Flegrei, Italy. *Journal of Geophysical Research: Solid Earth* 106 (B8), 16213–16221.
- Clauer, C., Huenges, E., 1995. Thermal Conductivity of Rocks and Minerals. *Rock Physics & Phase Relations: A Handbook of Physical Constants.* 3 pp. 105–126.
- Coats, R., Kendrick, J.E., Wallace, P.A., Miwa, T., Hornby, A.J., Ashworth, J.D., Lavallée, Y., 2018. Failure criteria for porous dome rocks and lavas: a study of Mt. Unzen, Japan. *Solid Earth* 9 (6), 1299–1328.
- Connor, C.B., Lichtner, P.C., Conway, F.M., Hill, B.E., Ovsyannikov, A.A., Federchenko, I., ... Taran, Y.A., 1997. Cooling of an igneous dike 20 yr after intrusion. *Geology* 25 (8), 711–714.
- Crank, J., 1979. *The Mathematics of Diffusion*. Oxford University Press.
- Crowley, J.K., Zimbelman, D.R., 1997. Mapping hydrothermally altered rocks on Mount Rainier, Washington, with airborne visible/infrared imaging spectrometer (AVIRIS) data. *Geology* 25 (6), 559–562.
- Currenti, G., Bonaccorso, A., Del Negro, C., Scandura, D., Boschi, E., 2010. Elasto-plastic modeling of volcano ground deformation. *Earth Planet. Sci. Lett.* 296 (3–4), 311–318.
- David, C., Menéndez, B., Darot, M., 1999. Influence of stress-induced and thermal cracking on physical properties and microstructure of La Peyratte granite. *Int. J. Rock Mech. Min. Sci.* 36 (4), 433–448.
- De Natale, G., Troise, C., Trigila, R., Dolfi, D., Chiarabba, C., 2004. Seismicity and 3-D substructure at Somma-Vesuvius volcano: evidence for magma quenching. *Earth Planet. Sci. Lett.* 221 (1–4), 181–196.
- Del Negro, C., Currenti, G., Scandura, D., 2009. Temperature-dependent viscoelastic modeling of ground deformation: application to Etna volcano during the 1993–1997 inflation period. *Phys. Earth Planet. Inter.* 172 (3–4), 299–309.
- Eggertsson, G.H., Lavallée, Y., Kendrick, J.E., Markússon, S.H., 2018. Improving fluid flow in geothermal reservoirs by thermal and mechanical stimulation: the case of Krafla volcano, Iceland. *J. Volcanol. Geotherm. Res.* <https://doi.org/10.1016/j.jvolgeores.2018.04.008>.
- Erbara, S., 1992. Thermal structure beneath Kuju volcano, central Kyushu, Japan. *J. Volcanol. Geotherm. Res.* 54 (1–2), 107–115.
- Esteban, L., Pimienta, L., Sarout, J., Delle Piane, C., Haffen, S., Géraud, Y., Timms, N.E., 2015. Study cases of thermal conductivity prediction from P-wave velocity and porosity. *Geothermics* 53, 255–269.
- Farquharson, J.I., Wild, B., Kushnir, A.R., Heap, M.J., Baud, P., Kennedy, B., 2019. Acid-Induced Dissolution of Andesite: Evolution of Permeability and Strength. *Journal of Geophysical Research: Solid Earth* 124 (1), 257–273.
- Fialko, Y.A., Rubin, A.M., 1999. Thermal and mechanical aspects of magma emplacement in giant dike swarms. *Journal of Geophysical Research: Solid Earth* 104 (B10), 23033–23049.
- Finn, C.A., Sisson, T.W., Deszcz-Pan, M., 2001. Aerogeophysical measurements of collapse-prone hydrothermally altered zones at Mount Rainier volcano. *Nature* 409 (6820), 600.

- Flörvént, Ó.G., Saemundsson, K., 1993. Heat flow and geothermal processes in Iceland. *Tectonophysics* 225 (1–2), 123–138.
- Fournier, N., Chardot, L., 2012. Understanding volcano hydrothermal unrest from geodetic observations: Insights from numerical modeling and application to White Island volcano, New Zealand. *Journal of Geophysical Research: Solid Earth* 117 (B11).
- Frolova, J., Ladygin, V., Rychagov, S., Zukhbayeva, D., 2014. Effects of hydrothermal alterations on physical and mechanical properties of rocks in the Kuril–Kamchatka island arc. *Eng. Geol.* 183, 80–95.
- Fujii, N., Osako, M., 1973. Thermal diffusivity of lunar rocks under atmospheric and vacuum conditions. *Earth Planet. Sci. Lett.* 18 (1), 65–71.
- Ghorbani, A., Revil, A., Coperey, A., Ahmed, A.S., Roque, S., Heap, M.J., ... Viveiros, F., 2018. Complex conductivity of volcanic rocks and the geophysical mapping of alteration in volcanoes. *Journal of Volcanology and Geothermal Research* 357, 106–127.
- Graham, I.J., Cole, J.W., Briggs, R.M., Gamble, J.A., Smith, I.E.M., 1995. Petrology and petrogenesis of volcanic rocks from the Taupo Volcanic Zone: a review. *J. Volcanol. Geotherm. Res.* 68 (1–3), 59–87.
- Griffiths, L., Lengliné, O., Heap, M.J., Baud, P., Schmittbuhl, J., 2018. Thermal cracking in Westerly Granite monitored using direct wave velocity, coda wave interferometry, and acoustic emissions. *Journal of Geophysical Research: Solid Earth* 123 (3), 2246–2261.
- Guéguen, Y., Palcauskas, V., 1994. *Introduction to the Physics of Rocks*. Princeton University Press.
- Guo, P.Y., Zhang, N., He, M.C., Bai, B.H., 2017. Effect of water saturation and temperature in the range of 193 to 373 K on the thermal conductivity of sandstone. *Tectonophysics* 699, 121–128.
- Gustafsson, S.E., 1991. Transient plane source techniques for thermal conductivity and thermal diffusivity measurements of solid materials. *Rev. Sci. Instrum.* 62 (3), 797–804.
- Gustavsson, M., Karawacki, E., Gustafsson, S.E., 1994. Thermal conductivity, thermal diffusivity, and specific heat of thin samples from transient measurements with hot disk sensors. *Rev. Sci. Instrum.* 65 (12), 3856–3859.
- Hackett, W.R., Houghton, B.F., 1989. A facies model for a Quaternary andesitic composite volcano: Ruapehu, New Zealand. *Bull. Volcanol.* 51 (1), 51–68.
- Hammerschmidt, U., Sabuga, W., 2000. Transient hot strip (THS) method: uncertainty assessment. *Int. J. Thermophys.* 21 (1), 217–248.
- Harlé, P., Kushnir, A.R., Aichholzer, C., Heap, M.J., Hehn, R., Maurer, V., ... Düringer, P., 2019. Heat flow density estimates in the Upper Rhine Graben using laboratory measurements of thermal conductivity on sedimentary rocks. *Geothermal Energy* 7 (1), 1–36.
- Harnett, C.E., Thomas, M.E., Purvance, M.D., Neuberg, J., 2018. Using a discrete element approach to model lava dome emplacement and collapse. *J. Volcanol. Geotherm. Res.* 359, 68–77.
- Harris, A.J., Stevenson, D.S., 1997. Thermal observations of degassing open conduits and fumaroles at Stromboli and Vulcano using remotely sensed data. *J. Volcanol. Geotherm. Res.* 76 (3–4), 175–198.
- Harris, A.J., Blake, S., Rothery, D.A., Stevens, N.F., 1997. A chronology of the 1991 to 1993 Mount Etna eruption using advanced very high resolution radiometer data: Implications for real-time thermal volcano monitoring. *Journal of Geophysical Research: Solid Earth* 102 (B4), 7985–8003.
- Heap, M.J., Kennedy, B.M., 2016. Exploring the scale-dependent permeability of fractured andesite. *Earth Planet. Sci. Lett.* 447, 139–150.
- Heap, M.J., Kolzenburg, S., Russell, J.K., Campbell, M.E., Welles, J., Farquharson, J.I., Ryan, A., 2014. Conditions and timescales for welding block-and-ash flow deposits. *J. Volcanol. Geotherm. Res.* 289, 202–209.
- Heap, M.J., Kennedy, B.M., Pernin, N., Jacquemard, L., Baud, P., Farquharson, J.I., Mayer, K., 2015. Mechanical behaviour and failure modes in the Whakaari (White Island volcano) hydrothermal system, New Zealand. *J. Volcanol. Geotherm. Res.* 295, 26–42.
- Heap, M.J., Violay, M., Wadsworth, F.B., Vasseur, J., 2017a. From rock to magma and back again: the evolution of temperature and deformation mechanism in conduit margin zones. *Earth Planet. Sci. Lett.* 463, 92–100.
- Heap, M.J., Kennedy, B.M., Farquharson, J.I., Ashworth, J., Mayer, K., Letham-Brake, M., ... Siratovich, P., 2017b. A multidisciplinary approach to quantify the permeability of the Whakaari/White Island volcanic hydrothermal system (Taupo Volcanic Zone, New Zealand). *Journal of Volcanology and Geothermal Research* 332, 88–108.
- Heap, M.J., Coats, R., Chen, C.F., Varley, N., Lavallée, Y., Kendrick, J., ... Reuschlé, T., 2018. Thermal resilience of microcracked andesitic dome rocks. *Journal of Volcanology and Geothermal Research* 367, 20–30.
- Heap, M.J., Troll, V.R., Kushnir, A.R.L., Gilg, H.A., Collinson, A.S.D., Deegan, F.M., Darmawan, H., Seraphine, N., Neuberg, J., Walter, T.R., 2019a. Hydrothermal alteration of andesitic lava domes can lead to explosive volcanic behaviour. *Nat. Commun.* <https://doi.org/10.1038/s41467-019-13102-8>.
- Heap, M.J., Kushnir, A.R., Gilg, H.A., Violay, M.E., Harlé, P., Baud, P., 2019b. Petrophysical properties of the Muschelkalk from the Soultz-sous-Forêts geothermal site (France), an important lithostratigraphic unit for geothermal exploitation in the Upper Rhine Graben. *Geothermal Energy* 7 (1), 27.
- Hofmeister, A., 2019. *Measurements, Mechanisms, and Models of Heat Transport*. Elsevier.
- Homand-Etienne, F., Houpert, R., 1989. Thermally induced microcracking in granites: characterization and analysis. *Int. J. Rock Mech. Min. Sci.* 26 (2), 125–134.
- Horai, K.I., 1991. Thermal conductivity of Hawaiian basalt: a new interpretation of Robertson and Peck's data. *Journal of Geophysical Research: Solid Earth* 96 (B3), 4125–4132.
- Horai, K.I., Simmons, G., Kanamori, H., Wones, D., 1970. Thermal diffusivity and conductivity of lunar material. *Science* 167 (3918), 730–731.
- Hurwitz, S., Ingebretsen, S.E., Sorey, M.L., 2002. Episodic thermal perturbations associated with groundwater flow: an example from Kilauea Volcano, Hawaii. *Journal of Geophysical Research: Solid Earth* 107 (B11).
- Hurwitz, S., Kipp, K.L., Ingebretsen, S.E., Reid, M.E., 2003. Groundwater flow, heat transport, and water table position within volcanic edifices: Implications for volcanic processes in the Cascade Range. *Journal of Geophysical Research: Solid Earth* 108 (B12).
- Hutchison, W., Varley, N., Pyle, D.M., Mather, T.A., Stevenson, J.A., 2013. Airborne thermal remote sensing of the Volcán de Colima (Mexico) lava dome from 2007 to 2010. *Geol. Soc. Lond., Spec. Publ.* 380 (1), 203–228.
- Irvine, T.N., 1970. Heat transfer during solidification of layered intrusions. I. Sheets and sills. *Can. J. Earth Sci.* 7 (4), 1031–1061.
- John, D.A., Sisson, T.W., Breit, G.N., Rye, R.O., Vallance, J.W., 2008. Characteristics, extent and origin of hydrothermal alteration at Mount Rainier Volcano, Cascades Arc, USA: Implications for debris-flow hazards and mineral deposits. *J. Volcanol. Geotherm. Res.* 175 (3), 289–314.
- Kant, M.A., Ammann, J., Rossi, E., Madonna, C., Höser, D., von Rohr, Rudolf, 2017. Thermal properties of Central Aare granite for temperatures up to 500 °C: irreversible changes due to thermal crack formation. *Geophys. Res. Lett.* 44 (2), 771–776.
- Kereszturi, G., Schaefer, L.N., Schleiffarth, W.K., Procter, J., Pullanagari, R.R., Mead, S., Kennedy, B., 2018. Integrating airborne hyperspectral imagery and LiDAR for volcano mapping and monitoring through image classification. *Int. J. Appl. Earth Obs. Geoinf.* 73, 323–339.
- Kranz, R.L., 1983. Microcracks in rocks: a review. *Tectonophysics* 100 (1–3), 449–480.
- Kühn, M., Stöfen, H., 2005. A reactive flow model of the geothermal reservoir Waiwera, New Zealand. *Hydrogeol. J.* 13 (4), 606–626.
- Kushnir, A.R., Martel, C., Bourdier, J.L., Heap, M.J., Reuschlé, T., Erdmann, S., ... Cholik, N., 2016. Probing permeability and microstructure: unravelling the role of a low-permeability dome on the explosivity of Merapi (Indonesia). *Journal of Volcanology and Geothermal Research* 316, 56–71.
- Lamur, A., Lavallée, Y., Iddon, F.E., Hornby, A.J., Kendrick, J.E., von Aulock, F.W., Wadsworth, F.B., 2018. Disclosing the temperature of columnar jointing in lavas. *Nat. Commun.* 9 (1), 1432.
- Lesparre, N., Gibert, D., Marteau, J., Komorowski, J.C., Nicollin, F., Coutant, O., 2012. Density muon radiography of La Soufrière of Guadeloupe volcano: comparison with geological, electrical resistivity and gravity data. *Geophys. J. Int.* 190 (2), 1008–1019.
- López, D.L., Williams, S.N., 1993. Catastrophic volcanic collapse: relation to hydrothermal processes. *Science* 260 (5115), 1794–1796.
- Marteau, J., Gibert, D., Lesparre, N., Nicollin, F., Noli, P., Giacoppo, F., 2012. Muons tomography applied to geosciences and volcanology. *Nuclear Instruments and Methods in Physics Research Section A: Accelerators, Spectrometers, Detectors and Associated Equipment* 695, 23–28.
- Mattsson, T., Burchardt, S., Almqvist, B.S., Ronchin, E., 2018. Syn-Emplacement Fracturing in the Sandfell Lacolith, Eastern Iceland—Implications for Rhyolite Intrusion Growth and Volcanic Hazards. *Front. Earth Sci.* 6, 5.
- Mercer, J.W., Faust, C.R., 1979. Geothermal reservoir simulation: 3. Application of liquid- and vapor-dominated hydrothermal modeling techniques to Wairakei, New Zealand. *Water Resour. Res.* 15 (3), 653–671.
- Mielke, P., Nehler, M., Bignall, G., Sass, I., 2015. Thermo-physical rock properties and the impact of advancing hydrothermal alteration—a case study from the Tauhara geothermal field, New Zealand. *J. Volcanol. Geotherm. Res.* 301, 14–28.
- Mielke, P., Weinert, S., Bignall, G., Sass, I., 2016. Thermo-physical rock properties of greywacke basement rock and intrusive lavas from the Taupo Volcanic Zone, New Zealand. *J. Volcanol. Geotherm. Res.* 324, 179–189.
- Mielke, P., Bär, K., Sass, I., 2017. Determining the relationship of thermal conductivity and compressional wave velocity of common rock types as a basis for reservoir characterization. *J. Appl. Geophys.* 140, 135–144.
- de Moor, J.M., Stix, J., Avard, G., Muller, C., Corrales, E., Diaz, J.A., ... Fischer, T.P., 2019. Insights on Hydrothermal-Magmatic Interactions and Eruptive Processes at Poás Volcano (Costa Rica) From High-Frequency Gas Monitoring and Drone Measurements. *Geophysical Research Letters* 46 (3), 1293–1302.
- Mordensky, S.P., Heap, M.J., Kennedy, B.M., Gilg, H.A., Villeneuve, M.C., Farquharson, J.I., Gravley, D.M., 2019. Influence of alteration on the mechanical behaviour and failure mode of andesite: implications for shallow seismicity and volcano monitoring. *Bull. Volcanol.* 81 (8), 44.
- Nabelek, P.J., Whittington, A.G., Hofmeister, A.M., 2010. Strain heating as a mechanism for partial melting and ultrahigh temperature metamorphism in convergent orogens: Implications of temperature-dependent thermal diffusivity and rheology. *Journal of Geophysical Research: Solid Earth* 115 (B12).
- Nabelek, P.J., Hofmeister, A.M., Whittington, A.G., 2012. The influence of temperature-dependent thermal diffusivity on the conductive cooling rates of plutons and temperature-time paths in contact aureoles. *Earth Planet. Sci. Lett.* 317, 157–164.
- Nagaraju, P., Roy, S., 2014. Effect of water saturation on rock thermal conductivity measurements. *Tectonophysics* 626, 137–143.
- Nara, Y., Meredith, P.G., Yoneda, T., Kaneko, K., 2011. Influence of macro-fractures and micro-fractures on permeability and elastic wave velocities in basalt at elevated pressure. *Tectonophysics* 503 (1–2), 52–59.
- Norton, D., Knight, J., 1977. Transport phenomena in hydrothermal systems: cooling plutons. *Am. J. Sci.* 277. <https://doi.org/10.2475/ajs.277.8.937>.
- Oppenheimer, C., Francis, P.W., Rothery, D.A., Carlton, R.W., Glaze, L.S., 1993. Infrared image analysis of volcanic thermal features: Lascar Volcano, Chile, 1984–1992. *Journal of Geophysical Research: Solid Earth* 98 (B3), 4269–4286.
- Petrunin, G.I., Yurehak, R.I., Tkach, G.F., 1971. Thermal diffusivity of Basalts at Temperatures from 300 to 1220 K. *Earth Phys.* 2, 65–68.
- Pimienta, L., Sarout, J., Esteban, L., Piane, C.D., 2014. Prediction of rocks thermal conductivity from elastic wave velocities, mineralogy and microstructure. *Geophys. J. Int.* 197 (2), 860–874.
- Pola, A., Crosta, G., Fusi, N., Barberini, V., Norini, G., 2012. Influence of alteration on physical properties of volcanic rocks. *Tectonophysics* 566, 67–86. <https://doi.org/10.1016/j.tecto.2012.07.017>.

- Popov, Y., Tertychnyi, V., Romushkevich, R., Korobkov, D., Pohl, J., 2003. Interrelations between thermal conductivity and other physical properties of rocks: experimental data. *Thermo-hydro-mechanical Coupling in Fractured Rock*. Birkhäuser, Basel, pp. 1137–1161.
- Reid, M.E., Sisson, T.W., Brien, D.L., 2001. Volcano collapse promoted by hydrothermal alteration and edifice shape, Mount Rainier, Washington. *Geology* 29 (9), 779–782.
- Robertson, E.C., Peck, D.L., 1974. Thermal conductivity of vesicular basalt from Hawaii. *J. Geophys. Res.* 79 (32), 4875–4888.
- Romine, W.L., Whittington, A.G., Nabelek, P.I., Hofmeister, A.M., 2012. Thermal diffusivity of rhyolitic glasses and melts: effects of temperature, crystals and dissolved water. *Bull. Volcanol.* 74 (10), 2273–2287.
- Rosas-Carbajal, M., Komorowski, J.C., Nicollin, F., Gibert, D., 2016. Volcano electrical tomography unveils edifice collapse hazard linked to hydrothermal system structure and dynamics. *Sci. Rep.* 6, 29899.
- Rosas-Carbajal, M., Jourde, K., Marteau, J., Deroussi, S., Komorowski, J.C., Gibert, D., 2017. Three-dimensional density structure of La Soufrière de Guadeloupe lava dome from simultaneous muon radiographies and gravity data. *Geophys. Res. Lett.* 44 (13), 6743–6751.
- Sammel, E.A., Ingebretsen, S.E., Mariner, R.H., 1988. The hydrothermal system at Newberry volcano, Oregon. *Journal of Geophysical Research: Solid Earth* 93 (B9), 10149–10162.
- Schauroth, J., Wadsworth, F.B., Kennedy, B., von Aulock, F.W., Lavallée, Y., Damby, D.E., ... & Dingwell, D.B. (2016). Conduit margin heating and deformation during the AD 1886 basaltic Plinian eruption at Tarawera volcano, New Zealand. *Bull. Volcanol.*, 78 (2), 12.
- Siratovich, P.A., von Aulock, F.W., Lavallée, Y., Cole, J.W., Kennedy, B.M., Villeneuve, M.C., 2015. Thermoelastic properties of the Rotokawa Andesite: a geothermal reservoir constraint. *J. Volcanol. Geotherm. Res.* 301, 1–13.
- Soueid Ahmed, A., Revil, A., Byrdina, S., Coperey, A., Gailler, L., Grobbe, N., ... Hogg, C., 2018. 3D electrical conductivity tomography of volcanoes. *Journal of Volcanology and Geothermal Research* 356, 243–263.
- Surono Jousset, P., Pallister, J., Boichu, M., Buongiorno, M.F., Budisantoso, A., Costa, F., ... Humaida, H., 2012. The 2010 explosive eruption of Java's Merapi volcano—a '100-year' event. *Journal of Volcanology and Geothermal Research* 241, 121–135.
- Tanaka, H.K., Taira, H., Uchida, T., Tanaka, M., Takeo, M., Ohminato, T., ... Tsujii, H., 2010. Three-dimensional computational axial tomography scan of a volcano with cosmic ray muon radiography. *Journal of Geophysical Research: Solid Earth* 115 (B12).
- Tsang, S., Lindsay, J., Coco, G., Wysocki, R., Lerner, G., Rader, E., Turner, G., Kennedy, B., 2019. The heating of substrates beneath basaltic lava flows. *Bull. Volcanol.* <https://doi.org/10.1007/s00445-019-1320-y>.
- Vélez, M.I., Blessent, D., Córdoba, S., López-Sánchez, J., Raymond, J., Parra-Palacio, E., 2018. Geothermal potential assessment of the Nevado del Ruiz volcano based on rock thermal conductivity measurements and numerical modeling of heat transfer. *J. S. Am. Earth Sci.* 81, 153–164.
- Vinciguerra, S., Trovato, C., Meredith, P.G., Benson, P.M., 2005. Relating seismic velocities, thermal cracking and permeability in Mt. Etna and Iceland basalts. *Int. J. Rock Mech. Min. Sci.* 42 (7–8), 900–910.
- Violette, S., Ledoux, E., Goblet, P., Carbone, J.P., 1997. Hydrologic and thermal modeling of an active volcano: the Piton de la Fournaise, Reunion. *J. Hydrol.* 191 (1–4), 37–63.
- Voight, B., Constantine, E.K., Sisowidjoyo, S., Torley, R., 2000. Historical eruptions of Merapi volcano, central Java, Indonesia, 1768–1998. *J. Volcanol. Geotherm. Res.* 100 (1–4), 69–138.
- Vosteen, H.D., Schellschmidt, R., 2003. Influence of temperature on thermal conductivity, thermal capacity and thermal diffusivity for different types of rock. *Physics and Chemistry of the Earth, Parts A/B/C* 28 (9–11), 499–509.
- Wadsworth, F.B., Vasseur, J., von Aulock, F.W., Hess, K.U., Scheu, B., Lavallée, Y., Dingwell, D.B., 2014. Nonisothermal viscous sintering of volcanic ash. *Journal of Geophysical Research: Solid Earth* 119 (12), 8792–8804.
- Wadsworth, F.B., Vasseur, J., Llewellyn, E.W., Genareau, K., Cimarelli, C., Dingwell, D.B., 2017. Size limits for rounding of volcanic ash particles heated by lightning. *Journal of Geophysical Research: Solid Earth* 122 (3), 1977–1989.
- Whittington, A.G., Hofmeister, A.M., Nabelek, P.I., 2009. Temperature-dependent thermal diffusivity of the Earth's crust and implications for magmatism. *Nature* 458 (7236), 319.
- Wilson, C.J.N., Houghton, B.F., McWilliams, M.O., Lanphere, M.A., Weaver, S.D., Briggs, R.M., 1995. Volcanic and structural evolution of Taupo Volcanic Zone, New Zealand: a review. *J. Volcanol. Geotherm. Res.* 68 (1–3), 1–28.
- Wooster, M.J., Wright, R., Blake, S., Rothery, D.A., 1997. Cooling mechanisms and an approximate thermal budget for the 1991–1993 Mount Etna lava flow. *Geophys. Res. Lett.* 24 (24), 3277–3280.
- Wright, R., Flynn, L.P., Garbeil, H., Harris, A.J., Pilger, E., 2004. MODVOLC: near-real-time thermal monitoring of global volcanism. *J. Volcanol. Geotherm. Res.* 135 (1–2), 29–49.
- Wyering, L.D., Villeneuve, M.C., Wallis, I.C., Siratovich, P.A., Kennedy, B.M., Gravley, D.M., Cant, J.L., 2014. Mechanical and physical properties of hydrothermally altered rocks, Taupo Volcanic Zone, New Zealand. *J. Volcanol. Geotherm. Res.* 288, 76–93. <https://doi.org/10.1016/j.jvolgeores.2014.10.008>.
- Zhu, W., Baud, P., Vinciguerra, S., Wong, T.F., 2016. Micromechanics of brittle faulting and cataclastic flow in Mount Etna basalt. *Journal of Geophysical Research: Solid Earth* 121 (6), 4268–4289.
- Zimmerman, R.W., 1989. Thermal conductivity of fluid-saturated rocks. *J. Pet. Sci. Eng.* 3 (3), 219–227.